Physics – Uspekhi **56** (8) 772 – 800 (2013)

REVIEWS OF TOPICAL PROBLEMS PACS numbers: 42.65.Ky, 42.79.Nv, 52.50.Jm

High-order harmonic generation in laser surface ablation: current trends

R A Ganeev

DOI: 10.3367/UFNe.0183.201308b.0815

Contents

Abstract. We review emerging concepts that have increased the efficiency of coherent XUV (extreme ultraviolet) generation through the use of laser frequency conversion in specially prepared plasmas and which have enabled high-order harmonic generation (HHG) spectroscopy to be used in spectral and structural analysis. We also present the current status of plasma HHG and examine what new trends have evolved in the field since it was reviewed last [*Phys. Usp.* 52 55 (2009)]. In particular, we consider new techniques for generating higher harmonics from various plasmas for the purpose of studying the physical properties of materials. It has been shown recently that HHG has application potential for many, sometimes unexpected, areas of laser radiation–matter interaction. It is argued that plasma HHG is — along with alternative coherent XUV generation — a powerful tool for a variety of spectroscopic and analytical applications.

R A Ganeev Imperial College London,
Prince Consort Road, SW7 2AZ London, United Kingdom
Tel. +44 (0) 20 75 94 76 41
E-mail: r.ganeev@imperial.ac.uk

Received 25 September 2012, revised 28 November 2012
Uspekhi Fizicheskikh Nauk **183** (8) 815 – 847 (2013)
DOI: 10.3367/UFNr.0183.201308b.0815
Edited by A Radzig

1. Introduction

Coherent short-wavelength radiation is of increasing importance for a broad spectrum of basic and applied research in various fields of physical, chemical, and life sciences. Among them, femtosecond time-resolved coherent diffractive imaging and photo-induced processes on surfaces and nanoparticles, as well as lithography, plasma diagnostics, and materials processing and diagnostics are of foremost interest. High-order harmonic generation (HHG) from femtosecond visible laser pulses allows producing coherent radiation in the extreme ultraviolet (XUV) spectral range. Table-top lasers render these processes possible with the prospect of widespread scientific applications. Until recently, a few gases were predominantly employed as target media for HHG. Other efforts relied on the creation of harmonics at solid surfaces, either by a coherent wake field excitation or, for petawatt-scale lasers, by a relativistically moving electron gas acting as a plasma mirror. So far, however, only low conversion efficiencies for HHG have been obtained, despite the enormous efforts. Other generation methods involve XUV free-electron lasers (FELs) and X-ray lasers.

To promote the use of XUV radiation, it therefore seems appropriate to advance laboratory scale sources to a higher application level. Many interesting experiments can be performed by HHG based on laboratory scale femtosecond lasers. These sources easily cover the spectral range between the 10- and 100-eV photon energy of the harmonics, and with few-cycle laser systems, even up to several hundred electron-

volts. For practical applications of high-order harmonic sources, higher conversion efficiency and, thus, an increase in the photon flux and the maximum photon energy of the harmonic radiation would be beneficial. HHG itself can be used as a spectroscopic tool for analysis of the optical, nonlinear optical, and structural properties of the harmonic generation emitters, presently comprising a few noble gases. The generation of higher harmonics in laser-produced plasmas from various solid-state targets, being for this purpose a relatively new and largely unexplored medium, promises to yield these advances.

Most interestingly, recent studies have shown that enhanced higher harmonics can also be generated from ablated nanoparticles, which opens the door to applications of local field enhancement, broad plasmon resonances, and more efficient recombination processes for plasma HHG. An increase in the harmonic output by quasiphase matching in specially prepared plasmas may be considered a very interesting prospect. For the plasma, a different and more flexible technique than used in neutral gases can be applied. The plasma may be spatially modified using a long pulse co-propagating with the fundamental driving pulse, and conditions might be found where quasiphase matching is possible over a long distance in the plasma, while the constructive and destructive interference of harmonic waves in such plasmas containing different emitters can provide new knowledge about the phase-related characteristics of this process. Thus, the above approach may be useful for producing an efficient source of short-wavelength ultra-short pulses for various applications and studies of the properties of harmonic emitters. Laser ablation-induced high-order harmonic generation spectroscopy is a new method for materials science and can be considered as one of the most important applications of HHG.

Previous reviews on plasma harmonic studies have mostly concentrated on the discussion of such specific topics as the application of nanoparticle-containing plasmas for HHG [1], the resonance-induced enhancement of harmonics [2], and applications of fullerenes as an attractive media for harmonic generation [3], contrary to the first two topical reviews published half a decade ago [4, 5], where a whole range of plasma HHG studies was presented. It seems timely to return back to the practice of showing a broad pattern of various developments in this field. It is also obvious that a comprehensive overview of the most recent findings can be useful for defining the next steps in the development of this relatively new and attractive area of material studies.

In this review, we discuss the realization of new ideas that have emerged over the last few years, and which have further improved HHG conversion efficiency through harmonic generation in specially prepared plasmas and allowed the spectral and structural studies of matter through plasma harmonic spectroscopy. We also present the current status of plasma HHG studies and show new trends and prospects in developing this field.

The layout of the paper is as follows. In Section 2, we outline the current status of plasma harmonic studies. New trends, schemes, and approaches in plasma HHG are presented in Section 3. Theoretical approaches for describing observed peculiarities of the higher harmonics in laser plasmas are discussed in Section 4. Harmonic generation using relatively long (picosecond) pulses converted in ablation-produced plasmas is considered in Section 5. Section 6 is concerned with the stable generation of higher harmonics of femtosecond laser radiation from laser-produced plasma plumes at a high (1 kHz) pulse repetition rate. In Section 7, a systematic analysis of harmonic radiation and plasma conditions during HHG in graphite-ablated plasma plumes using ultrashort laser pulses is presented from the standpoint of optimization of the frequency conversion of laser radiation. The first observations of isolated subfemtosecond XUV pulse generation in Mn-ablated plasmas are analyzed in Section 8. Short summary remarks made in Section 9 give some clues as to future developments and prospects in this interesting field of laser physics.

2. Current status of plasma HHG studies

High-order harmonic generation may presently be considered the simplest and most efficient technique for obtaining coherent short-wavelength radiation in a broad spectral range [6–14]. As was already mentioned, alternative means in this area are the employment of X-ray lasers [15, 16] and FELs [17]. However, unlike sources involving harmonic generation, X-ray lasers have been unable to generate radiation in a broad range of the extreme ultraviolet spectral domain. Other disadvantages of X-ray lasers involve their poor spatial coherence and radiation divergence. As regards FELs that generate radiation in the XUV spectral range, there are only a few such lasers. Furthermore, the application of these lasers is largely restricted by their extremely high development and maintenance cost.

HHG research is actively being pursued due to the availability of new high-power compact laser systems offering high output parameters (high pulse energy and intensity, and a high pulse repetition rate). Until recently, two mechanisms were utilized for HHG, namely, harmonic generation in gases [6, 8–12] and from surfaces [7, 13, 14]. The progress achieved in this area has enabled extending the range of generated coherent radiation toward the spectral region where the radiation can pass through water-bearing components (the so-called water window ranging from 2.3 to 4.6 nm [11, 12]). This circumstance is attractive from the standpoint of the practical implication of coherent short-wavelength radiation in studies of biological objects. However, data on the generation of such radiation obtained to date with the use of the above techniques have exhibited a low conversion efficiency to the XUV range (10^{-6} and below), which considerably limits their use in practice. This is supposedly the reason why in the last few years the emphasis has been focused on the optimization of another effect discovered in these investigations: the generation of attosecond pulses [18].

The search for ways of increasing the HHG efficiency in the XUV spectral range has long been (and still is) among the most relevant issues in optics. However, in the majority of cases, the conversion efficiency to high-order harmonics turns out to be insufficient for their use as real coherent short-wavelength radiation sources in biology, plasma diagnostics, medicine, microscopy, photolithography, XUV coherent diffraction imaging, time-resolved measurements, etc. The feasibility of increasing the intensities of high-order harmonics generated in gas jet sources by utilizing atomic and ion optical resonances has been studied primarily by theoretical methods [19, 20]. The results of a number of calculations suggest that the intensity of a harmonic may be substantially increased when this harmonic is at resonance with radiative transitions in the atomic and ion spectra of gases. This

approach, which has yet to be realized in gas HHG, may be an alternative (or a complement) to the method of wave phase matching for higher harmonics and laser radiation [11, 12].

The first experiments on HHG in the passage of laser radiation through the plasma produced on the surface of a solid target, carried out during first half of the nineties, turned out to be much less successful. As noted in a review on the properties of harmonics in plasmas, ''the effect of harmonic generation (in plasmas) calls for a more careful consideration and in-depth basic research'' [21]. Data obtained with the use of highly excited plasmas containing multiply charged ions revealed several limiting factors which did not permit generating the harmonics of a sufficiently high order and strong intensity [22–26]. Moreover, the harmonic intensity distribution did not follow the predictions of the so-called three-step model of HHG [27], according to which a plateau-like high-order harmonic intensity distribution (i.e., of approximately constant intensity) should be observed. Those studies, which were carried out in the mid-1990s, stopped at the demonstration of relatively low-order harmonics (from the 11th through the 25th). This disadvantage, as well as the low conversion efficiency, led to the erosion of interest in this HHG technique, especially in comparison with the achievements involving gas sources of HHG.

Nevertheless, there is reason to hope that harmonic intensities may be increased, and efficient shorter-wavelength coherent radiation may be obtained utilizing laser-produced plasmas. There are no fundamental limitations here: it only remains to find the optimal conditions for producing a plasma plume to serve as the efficient nonlinear medium for HHG. Laser-produced plasma may be validly used for this process if the effect of the limiting factors (self-defocusing, self-phase modulation, and wave phase mismatch of the harmonics and the radiation being converted) is minimized [22, 26]. Attention was drawn to this feature early in the study of lowest-order (third) harmonic generation in a weakly ionized plasma (see review [28]).

Among the special features of HHG in laser-produced plasmas, we first of all notify a wide range of nonlinear medium characteristics available by varying the conditions of laser plume production on the surface of a solid. This applies to plasma parameters such as the plasma dimension, the number density of ions, electrons, and neutral particles, and the degree of their excitation. The tapping of any elements of the Periodic Table that exist as solids largely extends the range of materials employed, together with thousands of complex solid-state samples, whereas only a few rare gases are typically used in gas HHG. Thus, the exploration of practically any available solid-state material through nonlinear spectroscopy comprising laser ablation and harmonic generation can be considered as a new tool for materials science.

In several cases, this method furnishes an opportunity to realize quasiresonance conditions for increasing the efficiency of single harmonic generation due to the effect of ion's optical transitions on the nonlinear response in the spectral range in question, thus allowing the studies of ionic transitions possessing strong oscillator strengths. This effect can hardly be observed in gas HHG because of a low probability of the coincidence of the atomic transition frequencies for few gases with the frequencies of single harmonics. The advantages of plasma HHG could largely be realized with the employment of low-excited and weakly ionized plasmas, because the limiting processes governing the dynamics of laser wavelength conversion would play a minor role under these conditions. This assumption has been confirmed by a diversity of studies concerned with high-order harmonic generation in the plasma media [29–33]. A substantial increase in the highest order of the generated harmonics, the observation of a long plateau and the emergence of a second plateau in the energy distribution of highest-order harmonics, the high conversion efficiencies obtained with several plasma formations, the realization of resonance enhancement of individual harmonics, the efficient harmonic enhancement from plasma plumes containing clusters of different materials, and other properties revealed in those and other studies [34–37] have demonstrated the advantages of utilizing specially prepared plasmas for HHG. The orders of higher harmonics obtained in plasma media to date range into the sixties and seventies [29, 31, 38, 39]. The highest-order harmonics (101st order, wavelength 7.9 nm) have been demonstrated in manganese plasmas [40]. The HHG conversion efficiency in the plateau region amounted to 10^{-5} [41]. In addition to that, the efficiency of conversion to an individual (resonantly enhanced) highest-order harmonic approached 10^{-4} [30, 31].

The quest for new plasma media that would favor the enhancement of an individual harmonic will enable further enhancement of harmonic conversion efficiency. The production of a single high-intensity harmonic (rather than a group of harmonics of equal, but greatly weaker, intensity in the plateau region) would open up the way to the practical implication of these coherent short-wavelength radiation sources, without using the dispersive elements (gratings) for the separation of a given radiation. Resonantly enhanced individual harmonics observed in several plasma media allowed expecting that similar features will be discovered for other plasma formations. The wavelength of a generated harmonic may then be tuned to a transition with a higher oscillator strength by tuning wavelength of the driving laser [30, 36], as well as by varying the chirp of the laser radiation [31, 33, 35]. The application of ablated nanoparticles and clusters for HHG can also enhance the yield of harmonics in the XUV range. Further improvements in HHG conversion efficiency and the extension of the number of generated harmonics require a systematic study of the influence of various plasma and laser parameters on ablation harmonics. Many new peculiarities of plasma plume-generated harmonics have emerged over the last few years [42–74], allowing the expectation of further extension of our knowledge about material properties applying this novel powerful method of nonlinear spectroscopy.

Whilst the first stage of these successful studies was entirely focused on improvements in the harmonic yield from plasma, at the current stage of knowledge of higher-order nonlinear optical processes in ablation plumes, one can consider this method as a new tool for materials science. Thus, the search for the dual role of plasma HHG as a method for efficient coherent XUV light generation and of material probing is a milestone of further developments in this field. Below, we show new trends that have emerged during recent years, which demonstrate the attractiveness of this method.

3. Recent trends, schemes, and approaches in plasma HHG

Plasma HHG has considerably matured over the last few years and continues to attract the growing attention of

various laboratories worldwide. Currently, studies of plasma HHG are being carried out in Japan, Canada, India, Uzbekistan, the USA, Ireland, Germany, Korea, Spain, and the United Kingdom. Below, the most recent developments and some fresh approaches, experimental schemes, and ideas are described, which could considerably push this field toward the dramatic improvement in the output characteristics of harmonics and a better understanding of the properties of matter through plasma HHG spectroscopy.

Intense HHG from plasma that is created at the surface of different carbon targets was demonstrated recently in paper [62] using a 10-Hz pulse repetition rate laser. A high-order harmonic energy in the multimicrojoule range for each harmonic order from the 11th to the 17th was obtained. It was concluded, by analyzing the target morphology and the plasma composition, that the intense harmonics from the bulk carbon targets originate from the nanoparticles produced during ablation of the carbon-containing target. It was shown in previous work [37] that nanoparticles and films composed of C_{60} molecules would generate harmonics that are more intense than those obtained from solid targets. The disadvantage of using nanoparticle and film targets is the instability of the harmonics, which considerably vary from shot to shot, and even disappear after a few laser shots if the target is not displaced. On the contrary, it was found in Ref. [62] that carbon bulk targets can generate harmonics comparable in intensity to those from nanoparticles or C_{60} plasma targets.

A scanning electron microscope (SEM) image of plasma debris from a carbon target revealed that the plasma plumes contain nanoparticles with sizes varying between 100 and 300 nm. It was therefore suggested that, during the interaction of the heating pulse with the carbon target, nanoparticles are formed in the plasma and are then pumped by the fundamental pulse to induce the generation of harmonics. The harmonic intensity reached by using a bulk carbon target remained stable for several minutes, even without displacing the target position. By creating the plasma for 5 min at the same place of the solid carbon target, the harmonic intensity did not decrease more than 10%, while that from nanoparticles decreased more than 90% within a few seconds after laser irradiation. It was also noted that, unlike most other solid targets, the highest harmonic order obtained with a carbon target does not exceed 21. According to the cut-off law of the plateau harmonic spectrum defined by the three-step model, it was suggested that these harmonics are generated by neutral atoms, rather than ions, as in the case of other solid targets.

Further improvements in both the stability of carbon-containing plasma harmonics and their enhanced yield were reported in paper [63]. The importance of these parameters is determined by the applicability of converted radiation for various needs. Much effort has been dedicated to the refinement of these characteristics during the long history of studying harmonic generation in gases. Multimicrojoule harmonics have been generated by the energy scaling of gas HHG under highly optimized conditions [75, 76], which, however, have basically pushed gas HHG to its limits. Therefore, an urgent demand was created for a search for the methods to generate even more intense harmonics and attosecond light pulses. For these purposes, gas clusters [77] and plasma produced from nanoparticle targets [37, 78] can be examined to increase the intensity of harmonics. In the former case, microjoule intense harmonics have been demonstrated in the range of 50–90 nm.

However, as was mentioned above, nanoparticle targets run against the problem of a rapid decrease in the HHG intensity with consecutive shots, which prevents them from being used in applications, especially in the case of high pulse repetition rate lasers. These exotic targets are also not always available in abundance. A new approach has been reported recently, which showed that highly efficient and stable high-order harmonics could be generated from a target that is readily available in the household: pencil lead of a mechanical pencil [63]. The energy measurements of the harmonics generated from plasma produced from pencil lead and their comparison with harmonics produced from C_{60} particles, which have proven to be one of the most efficient media for plasma HHG, showed the advantages of harmonics emerged from the former medium. The important advantage of using a pencil lead target is the shot-to-shot stability of the harmonic intensity over a sufficiently large number of laser shots.

To understand the uniqueness of the pencil lead plasma, researchers exploited an SEM to analyze the ablated material debris deposited on silicon substrates that were placed nearby the ablation plume. Those SEM images revealed that the plasma created from a pencil lead target contains nanoparticles whose mean size was close to about 200 nm. They therefore suspected that, due to the ablation of the pencil lead target by the heating pulse, the nanoparticles were formed on the target surface and remained in the plasma, which in turn led to the generation of the intense harmonics.

From the experimental observations of stronger harmonics compared with fullerene plasma and the morphology of plasma debris, the authors of Refs [62, 63] inferred that the origin of the extremely strong harmonics from pencil lead and carbon plasmas is similar to those described for nanoparticle targets. The presence of nanoparticles in the plasma deposition and low cut-off suggest that neutral atoms of nanoparticles are the main source of intense harmonics from the pencil plasma. An explanation for intense harmonic generation from nanoparticles could be the higher concentration of neutral atoms due to the presence of nanoparticles. Unlike isolated atoms and ions, whose densities quickly decrease due to plasma expansion, the nanoparticles retain densities that are close to those in a solid state. Combined with the higher harmonic efficiency of neutral atoms than that of their ions, the neutral atoms within the nanoparticle could efficiently generate high-order harmonics. The authors of Refs [62, 63] estimated a conversion efficiency at a level of $\sim 10^{-4}$ for harmonics in the plateau range.

The important issue of HHG from plasmas is related to the characteristics of the generated harmonics. Whereas the conversion efficiency issue has been taken seriously in recently developing this technique, which led to a considerable enhancement of harmonic pulse energy, no temporal characterization of plasma harmonic pulses had been performed until recently. This is a crucial element for applications of a new source of coherent XUV radiation. It should not be taken for granted that this harmonic emission has a nice attosecond structure. Indeed, the harmonic generation in plasma induces many sources of distortion: the higher electron densities and gradients will affect the generation of harmonics through phase mismatching and may result in distortion of both the harmonic spatial phase-front and the spectral phase. Furthermore, the temporal characterization itself raises issues, such as probe beam distortions, target deterioration, and the instability of harmonic intensity.

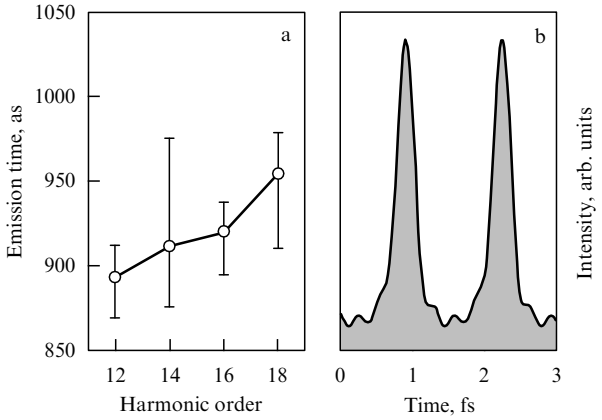

Figure 1. (a) Emission times and (b) temporal intensity profile of pulses corresponding to the harmonic order between 11 and 19 [62].

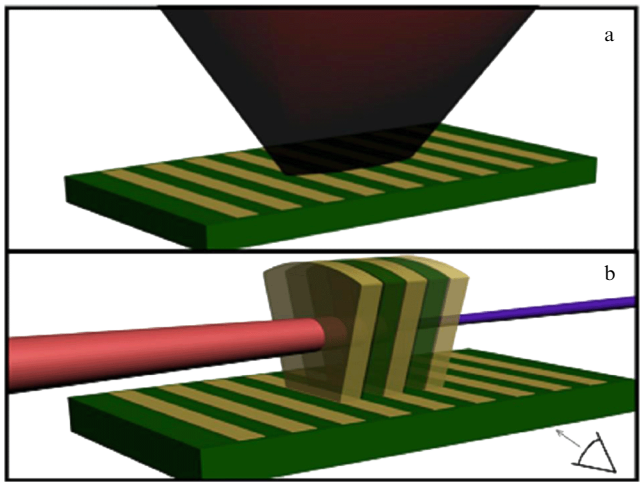

Figure 2. Schematics of the experiment: (a) a lithographic pattern hit by a relatively low-intensity laser beam, and (b) the formed plasma jets in which a high-intensity laser pump facilitates HHG [82].

The first measurements of the attosecond emission generated from underdense plasma produced on a solid target were reported by Elouga Bom et al. [62]. They generated high-order harmonics of a femtosecond infrared (IR) Ti:sapphire laser focused onto a weakly ionized chromium plasma. The characterization of the plasma attosecond emission was performed using the RABITT technique [79]. The measurement of the harmonic spectral amplitude and phase allows direct access to the attosecond structure through a Fourier transform. The amplitude of each harmonic is easily given by the amplitude of the main photoelectron lines corrected with due regard for the ionization cross section.

The relative phase between neighboring order harmonics is accessed through two-photon XUV + IR ionization of the target gas. When the IR beam is superimposed on the XUV beam in argon gas, sidebands appear in the photoelectron spectrum between the main lines. They correspond to two-photon transitions: absorption of a harmonic photon with the frequency $q\omega_0$ (q is the harmonic number), accompanied by either absorption or stimulated emission of a laser photon with ω_0. Since two coherent quantum paths lead to the same sideband, interferences occur, which result in an oscillation of the sideband amplitude as the delay time τ between the IR and harmonic field is scanned with sub-IR-laser-cycle resolution. The phase of the oscillation is the phase difference between the two interfering paths. The phase difference, $\varphi_q - \varphi_{q+2}$, between two consecutive harmonics can then be extracted, readily giving the group delay, also called emission time. From the phases φ_q obtained by integrating the emission times and the amplitudes A_q of the order-varying harmonics, one can reconstruct the temporal intensity profile.

The result for the measured five harmonic orders from $q = 11$ to $q = 19$ is shown in Fig. 1. The reconstructed temporal profile of the harmonic emission forms an attosecond pulse train, each pulse being 300 as in duration [full width at half maximum (FWHM)]. Assuming all five harmonics to be in phase, one can obtain the shortest pulses possible, i.e., the Fourier-transform limited pulses. The corresponding duration is $\tau = 285$ as. The measured duration of 300 as is thus only 1.05 times the Fourier-transform limited duration.

In the standard scheme of gas HHG, an ultrashort laser pump beam at intensities above 10^{14} W cm^{-2} is focused onto a gas jet, generating higher harmonics. The yield of such schemes is inevitably limited by dispersion in the medium. Across a distance equal to the coherence length, a phase mismatch of π grows and causes destructive interference between the pump and high-harmonic beams. This process is one of the major limitations on the conversion efficiency of HHG. Quasiphase matching (QPM) is a well-known approach for resolving this phase mismatch problem [80]. In QPM, the medium is modulated with a coherence length period, so that the pump phase or harmonic emission is changed to prevent the destructive interference caused by the phase mismatch. For HHG in the XUV range and beyond, dispersion in the medium can be mostly attributed to free electrons generated in the course of the laser ionization of the medium. Under this assumption, the coherence length (at 0.8-μm laser wavelength) is given (in meters) by $L_c \propto 10^{15}/qN_e$, where N_e is the free electron density [cm^{-3}], and q is the harmonic number. Previously, QPM was realized by using multiple gas jets whose pressure and separation were properly controlled [81]. However, the realization of this technique is limited by geometrical constraints on the number and minimal separation of the jets.

It was proposed that the same procedure could be established for plasma HHG [82] using a simple method for producing numerous plasma jets tailored for the HHG, relieving technical restraints on the dimensions of the jets and their periodicity. In this scheme, the jets are produced by ablation of a microlithographic periodic stripe pattern (Fig. 2). Cylindrical plasma jets formed by ablation extend the lithographic pattern into the space above the target, creating a row of narrow plasma jets with a different material composition. The efficiency of HHG in plasma has been demonstrated to vary considerably with the atomic composition [38], and the periodic change in this efficiency enables QPM-HHG.

The results of work [82] demonstrate a simple method for generating periodic plasma structures by ablating a lithographic pattern. When passing a high-intensity laser pulse through such plasma patterns, suitable conditions for the QPM, required for HHG, can be created. These measurements suggest that such conditions exist between 140 and 180 ns after the plasma initiation by the ablating laser pulse (Fig. 3). Within this temporal window, the plasma jets are

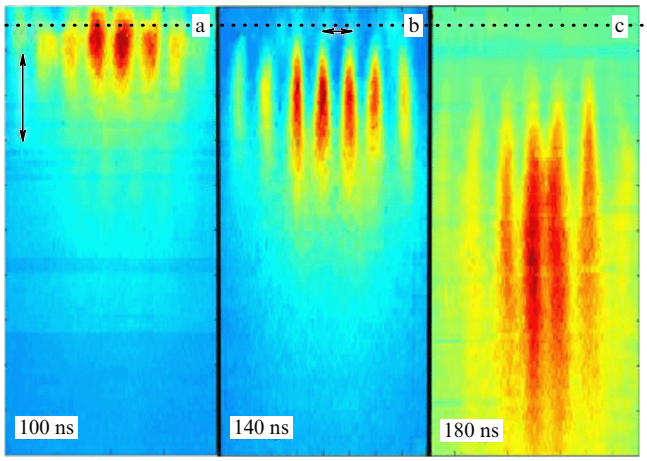

Figure 3. Monochromatic imaging of the plasma jets at different times: (a) 100, (b) 140, and (c) 180 ns, using a 30 ns gate. The dashed line marks the target's surface, and the double arrows measure up to 200 μm scale [82].

several hundred microns wide and have a relatively uniform temperature and a relatively low electron density of $\sim 10^{17}$ cm^{-3}, whereas at later times the plasma structure begins to fade. Examining Fig. 3 in depth shows that the modulation of the plasma density is significant for harmonic generation, while the authors suggest that much higher periodicities suitable for the generation of higher harmonics could be reached by using finer lithography in preparation of the target. They have demonstrated the feasibility of a robust scheme for tailoring plasma structures with control over material composition, temperature and density (of both free electrons and neutrals), through the ablation of specifically prepared lithographic targets, which can support quasiphase matched HHG.

4. Theoretical studies of high-order harmonic generation in various media

4.1 Harmonic generation in fullerenes using few-cycle pulses

Fullerenes can be considered as an attractive nonlinear medium for HHG. Their relatively large sizes and broadband surface plasmon resonance (SPR) in the extreme ultraviolet range allowed the first demonstration of efficient HHG from fullerenes near their SPR ($\lambda_{\mathrm{SPR}} \approx 60$ nm, with 10-nm FWHM) [37]. The application of the laser ablation technique led to the creation of relatively dense C_{60}-rich plasma ($\sim 5 \times 10^{16}$ cm^{-3}), in stark contrast to the density $< 10^{14}$ cm^{-3} obtained using heat oven-based methods of production of fullerene beams.

Theoretical studies of HHG from C_{60} using multicycle pulses involved extending the three-step model [83], analyzing an electron constrained in its motion to the surface of a rigid sphere with geometrical parameters similar to those of the C_{60} fullerene [84], and applying dynamical simulations [85]. In the last study, higher-order harmonics were shown to appear due to multiple excitations and could be easily generated even with a weak laser field. Those studies revealed how HHG can be utilized to probe the electronic and molecular structure of C_{60}. At the same time, the theoretical investigation of such systems is hampered by the fact that the Hamiltonian governing HHG is time-dependent, and the systems consist of many electrons. The investigation of the influence of the fundamental properties of electrons on resonant HHG can be performed by means of the multiconfigurational time-dependent Hartree–Fock (MCTDHF) approach which has the accuracy of the direct numerical solution to the Schrödinger equation and is almost as simple as the ordinary time-dependent Hartree–Fock (TDHF) approach. In particular, the computations might be based on Heidelberg multiconfigurational time-dependent Hartree (MCTDH) software packages [86]. In paper [49], simulations of resonant HHG were performed by means of an MCTDHF approach for three-dimensional fullerene-like systems. The influence of the C_{60} SPR on the harmonic generation efficiency in the range of 60 nm ($E = 20$ eV) was analyzed and showed ways to optimize resonant HHG.

The saturation intensities of different charge states of C_{60} are higher than in isolated atoms of a similar ionization potential [87]. In this connection, it would be interesting to analyze the behavior of fullerene molecules in the field of a few-cycle laser pulses from the point of view of harmonic generation and compare these studies with those carried out using multicycle pulses.

Once considered exotic, fullerenes are nowadays commonly synthesized and utilized in research. These molecules have a graphite-like structure but, instead of a purely hexagonal packing, they also contain pentagons (or even heptagons) of carbon atoms, which bend the graphene sheet into spheres, ellipses, or cylinders. Among fullerenes, C_{60} molecule is particularly noteworthy, since its pentagonal and hexagonal rings of carbon atoms give it a spherical shape. This feature endows C_{60} with an appealing spherical symmetry, which can be taken into account to simplify the treatment [88]. Here, we briefly outline the theory of a C_{60} molecule driven by a laser pulse in the form $E(t) = E_0(t) \sin(\omega_{\mathrm{L}} t)$, polarized in the z-direction with $E_0(t)$ describing the on–off switching of the pulse profile and frequency ω_{L}; in the present calculations, the pulse profile has always been taken as trapezoidal with 2 optical cycles of switching on and off.

The C_{60}–laser field interaction will be described in the single active electron approximation with one electron constrained to a structureless, spherical surface with a radius $R = 3.55 \times 10^{-8}$ cm $= 6.71 a_0$, where a_0 is the Bohr radius; the electron is otherwise unconstrained.

Within the model considered, the Hamiltonian of the problem is written out as

$$\hat{H} = \hat{H}_0 + \hbar\Omega_0(t) \cos\theta \sin(\omega_{\mathrm{L}} t)\,, \tag{1}$$

where

$$\hat{H}_0 = \frac{\hbar^2}{2I}\,\hat{L}^2 \tag{2}$$

is the Hamiltonian of C_{60} in the absence of a laser field, $\hbar\Omega_0(t) = eRE_0(t)$, $I = m_{\mathrm{e}}R$ is the moment of inertia of the electron, and $\hat{L}^2$ is the angular momentum operator squared, whose eigenstates are the usual spherical harmonics $Y_{\ell m}(\theta, \varphi) \rightarrow |\ell, m\rangle$: $\hat{L}^2|\ell, m\rangle = \ell(\ell+1)|\ell, m\rangle$, where ℓ is the orbital angular momentum, and m is the quantum number of the angular momentum projection. Nevertheless, the fact that φ is a cyclic variable makes m a constant quantum number; θ is the angle the electron position vector takes with

the z-axis. Accordingly, the energies of the bare states are

$$\hbar\omega_\ell \equiv \frac{\hbar^2}{2I}\,\ell(\ell+1); \tag{3}$$

thus, the gap between adjacent energy levels linearly increases with λ. This particular feature can be reminiscent of the ionization suppression in C_{60} resulting from the experimental fact that the molecule can absorb from the laser field an amount of energy quite larger than the minimum required for its ionization.

The time-dependent Schrödinger equation to be solved is written in the form

$$\mathrm{i}\hbar\,\frac{\partial}{\partial t}\,\big|\Psi(t)\big\rangle = \hat{H}\big|\Psi(t)\big\rangle\,, \tag{4}$$

with $|\Psi(t)\rangle$ being the full time-dependent wave function of the active electron acted upon by the laser field.

In accordance with previous assumptions, it is convenient to write out the state vector at time t, $|\Psi(t)\rangle$, as a linear combination of eigenstates of the laser-free Hamiltonian $\hat{H}_0$:

$$\big|\Psi(t)\big\rangle = \sum_{\ell'=0}^{\infty}\sum_{m'=-\ell}^{\ell} a_{\ell',m'}(t)|\ell',m'\rangle\,, \tag{5}$$

where $a_{\ell',m'}(t)$ are expansion coefficients to be found by substitution into the time-dependent Schrödinger equation. Let $|\Lambda,m\rangle$ be the initial state for the highest-occupied molecular orbital; according to the previous discussion, the laser field will couple only states with $m=m'$. Therefore, the time-dependent Schrödinger equation becomes

$$\mathrm{i}\dot{a}_{\ell,m} = \omega_\ell\, a_{\ell,m} + \Omega_0 \sum_{\ell'=\Lambda}^{\infty} \sin(\omega_\mathrm{L}t)\langle\ell,m|\cos\theta|\ell',m\rangle a_{\ell',m}\,. \tag{6}$$

When fulfilling the Pauli exclusion principle and the single active electron approximation, the summation does not extend over occupied molecular core states. Thus, the matrix element calculation reduces to a standard integration of three spherical harmonics:

$$\langle\ell,m|\cos\theta|\ell',m\rangle = \sqrt{\frac{4\pi}{3}}\int Y^*_{\ell,m}(\theta,\varphi)\,Y_{1,0}(\theta,\varphi)\,Y_{\ell',m}(\theta,\varphi)\,\mathrm{d}\Omega\,. \tag{7}$$

By setting

$$b_{\ell,m} \equiv \sqrt{\frac{(\ell+m+1)(\ell-m+1)}{(2\ell+1)(2\ell+3)}}, \tag{8}$$

one can obtain:

if $\ell \geqslant \Lambda$ then

$$\int Y^*_{\ell,0}(\theta,\varphi)\,Y_{1,0}(\theta,\varphi)\,Y_{\ell+1,m}(\theta,\varphi)\,\mathrm{d}\Omega = \sqrt{\frac{3}{4\pi}}\,b_{\ell,m}\,; \tag{9}$$

if $\ell > \Lambda$ then

$$\int Y^*_{\ell,0}(\theta,\varphi)\,Y_{1,0}(\theta,\varphi)\,Y_{\ell-1,m}(\theta,\varphi)\,\mathrm{d}\Omega = \sqrt{\frac{3}{4\pi}}\,b_{\ell-1,m}\,.$$

Therefore, one arrives at

$$\begin{aligned}
&\mathrm{i}\dot{a}_{\Lambda,m} = \omega_\Lambda a_{\Lambda,m} + \Omega_0(t)\,b_{\Lambda,m}\sin(\omega_\mathrm{L}t)\,a_{\Lambda+1,m}\,,\\
&\mathrm{i}\dot{a}_{\ell>\Lambda,m} = \omega_\ell\,a_{\ell,m} + \Omega_0(t)\sin(\omega_\mathrm{L}t)(b_{\ell-1,m}a_{\ell-1,m} + b_{\ell,m}a_{\ell+1,m})\,.
\end{aligned} \tag{10}$$

Since the energy gap increases with ℓ, one can argue that the population of the upper levels becomes negligible; thus, the energy levels with quantum numbers $\ell > \Lambda + N$ do not participate in the dynamics of the system. The set of differential equations shows a ladder-like structure, so that any energy level is coupled to the two adjacent levels. This system can be numerically solved by utilizing the Odesolve45 Matlab numerical routine.

Once the probability amplitudes $a_{k,m}$ have been obtained, it is rather simple to get the matrix element of the electric dipole moment $er(t)$ induced by the laser field on C_{60}:

$$\begin{aligned}
r(t) &= \big\langle\Psi(t)\big|R\cos\theta\big|\Psi(t)\big\rangle\\
&= R\sum_{s=0}^{\infty} b_{\Lambda+s,m}[a^*_{\Lambda+s,m}a_{\Lambda+s+1,m} + a_{\Lambda+s,m}a^*_{\Lambda+s+1,m}]\,.
\end{aligned} \tag{11}$$

Here, R is the fullerene radius.

The calculated harmonic spectra from C_{60} molecules are presented in Fig. 4 for 780-nm (photon energy $E_\mathrm{ph} = 1.6$ eV) and 1300-nm (photon energy $E_\mathrm{ph} = 0.96$ eV) laser pulses propagating through a fullerene medium [89]. The calculations were carried out for 2-cycle pulses ($t = 5.2$ fs) and 12-cycle pulses ($t = 31$ fs) of 780-nm radiation, and 8-cycle pulses ($t = 34$ fs) of 1300-nm radiation and an intensity of 6×10^{14} W cm^{-2}, which was close to the experimental conditions of fullerene HHG [37, 89].

The spectra of well-resolved harmonics (see Fig. 4) are formed but with broadened lines (in the case of short laser pulses) and hyper-Raman lines (in the case of long pulses) presented. Hyper-Raman lines with a frequency other than the harmonic frequencies are due to transitions between laser-dressed molecular states [90, 91]. The presence of these lines was predicted at the very beginning of the HHG theoretical treatment [92] and has been found in different contexts, such as the two-level approximation, quantum dot calculations, the hydrogen-like approximation, and so on [93–96], but has never been observed in actual experiments. Several explanations have been proposed for this failure; for example, it has been argued that they add destructively in the forward wave direction or that they show a transient nature and are thus overwhelmed by the odd harmonics presented [97, 98].

Calculations have shown the presence of well-defined harmonics (up to the limiting generated harmonic order $H_\mathrm{c} = 31$) in the case of 1300-nm multicycle pulses. This theoretical model exploited the spherical symmetry of the C_{60} molecule by introducing a number of approximations, the most important of which is that the molecule cannot be ionized. This approximation deserves some comment. In spite of the ionization suppression of the C_{60} molecule, some ionization is bound to occur, so that the theory becomes unreliable when ionization becomes significant. The plateau harmonic cut-off in the case of 1300-nm radiation was extended, as opposed to 780-nm radiation ($H_\mathrm{c} = 17$), attesting to agreement with experiment [89].

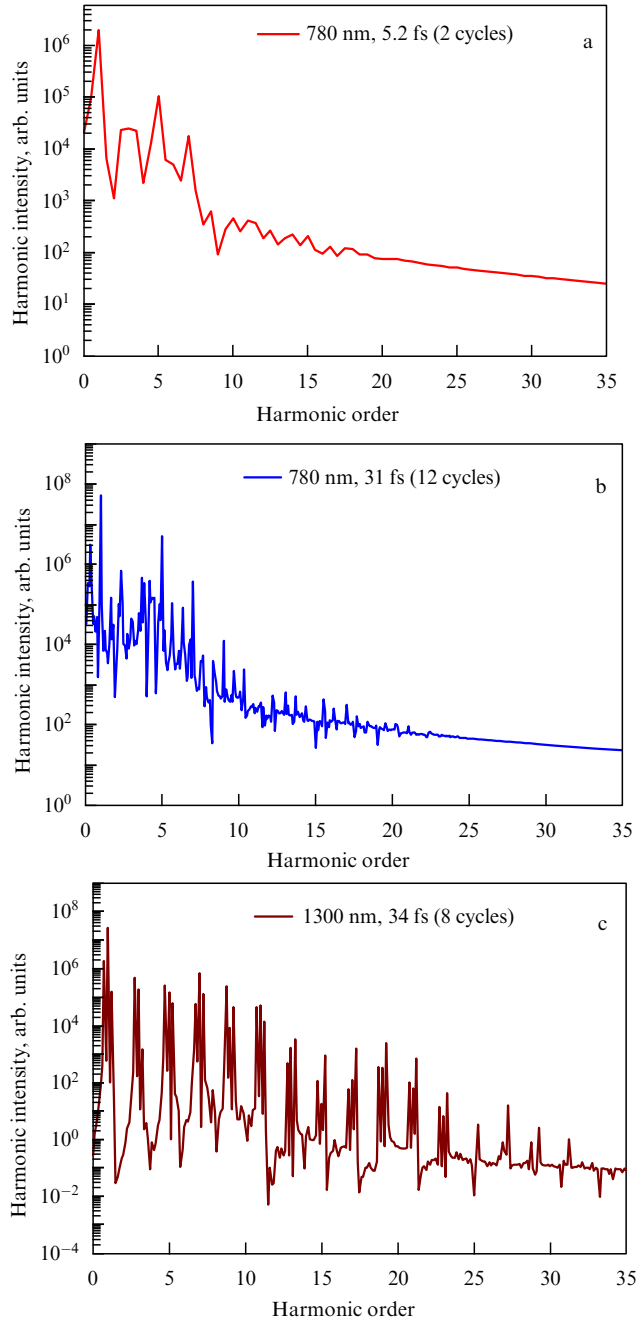

Figure 4. Calculated harmonic spectra obtained from fullerene plasma in the case of (a, b) 780-nm and (c) 1300-nm probe radiation at the intensities of 6×10^{14} W cm^{-2}. The pulse durations are (a) 2 optical cycles (5.2 fs), (b) 12 optical cycles (31 fs), and (c) 8 optical cycles (34 fs) [89].

4.2 Various approaches to describing observed peculiarities of the resonant enhancement of a single harmonic in laser plasma

The dependence of the recombination probability on the electron return energy and on the structure of the target is reflected in the HHG spectrum and has been a subject of intensive research in recent years. To enhance the notoriously low efficiency of the HHG process, it appears promising to exploit the effect of resonances, which is known to be of great importance in photoionization. The investigation of resonant peaks in the photoionization cross section has a long history, including studies of autoionizing resonances [99, 100], shape resonances [101], and giant resonances [102], but there have been only a few experimental studies on the role of resonances in HHG.

The role of atomic resonances in increasing the laser radiation conversion efficiency was actively discussed in the framework of perturbation theory at the early stages of the study of low-order harmonic generation (see monograph [103] and references cited therein). In the case of HHG, the increase in the efficiency of generated harmonics due to resonance processes came under discussion almost a decade ago, and this approach appears to have considerable promise with the use of ion and, in some cases, atomic resonances [19, 20, 104–108]. These papers comprise both the theoretical treatment of the process and the description of the first attempts to form resonance conditions in gas HHG experiments. In particular, the authors of Ref. [19] investigated resonance-enhanced HHG, with emphasis placed on the physical mechanisms of the enhancement. By truncating a long-range interaction potential, the researchers studied the significance of the long-range tail, the Rydberg series, and the existence of highly excited states for the enhancements of harmonics.

While theoretical estimates testify to the possibility of an efficient enhancement of individual harmonics and groups of harmonics, experimental work revealed the difficulties encountered in observation of resonantly enhanced HHG in gases. Further developments have demonstrated that the use of plasma media could largely facilitate the solution to the problem of resonance harmonic enhancement. Examination of a large group of potential targets allowed identification of some of them as suitable for demonstrating this process [2, 33]. The advantages of 'plasma HHG' over 'gas HHG' were amply manifested in those studies, because the number of possible media in the former case is far greater than in the latter case.

Some attempts at explaining the experimental observations of resonant enhancement in plasma harmonics have been reported recently [49, 55, 109–114]. In particular, it has been shown in Ref. [110] that the influence of atomic autoionizing states on the phase matching of HHG may result in the efficient selection of a single harmonic in calcium-ablated plasma. This was the first report on efficient high-order harmonic selection using autoionizing states. The calculations [110] showed that the achievement of phase matching for the HHG with Ti:sapphire laser radiation in Ca^+ plasma results in the selection of a single (21st) harmonic with a conversion efficiency of $\sim 10^{-3}$. The variations of the plasma components and fundamental wavelength result in the tuning of a selected harmonic frequency in the plateau region. The influence of a nonstationary Stark shift and free electrons changes the phase mismatch and the optimal laser frequency at which the efficient selection of a single harmonic is achieved. Therefore, intensity enhancement due to laser beam propagation effects can be even greater than that in the single-atom approximation.

An approach that suggests an HHG model describing enhancement of the generation efficiency for the harmonic resonant with the optical transition between the ground and the autoionizing state of the generating ion was developed by Strelkov [111]. In his model, the third (recombination) step of the HHG three-step scenario [27] is partitioned into two steps: the capture of a laser-accelerated electron into an autoionizing state of the parent ion, followed by the radiative relaxation of this state to the ground state with emission of the harmonic photon. Figure 5 illustrates calculated results from

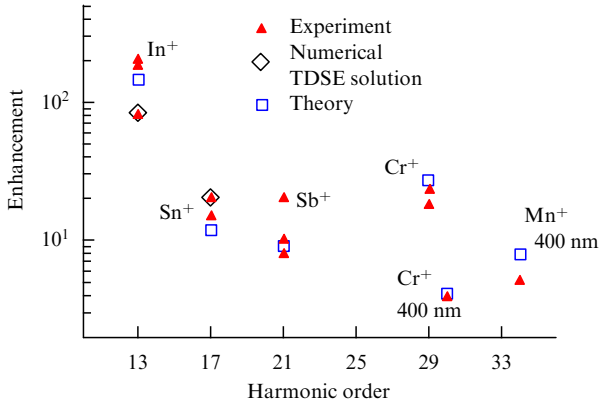

Figure 5. Comparison of experimental data on resonant enhancement of harmonics with analytical and numerical results obtained using time-dependent Schrödinger equation solutions [111].

paper [111] indicating that while the enhancement values for different media differ by almost two orders of magnitude, the theoretical results are close to the experimental ones. The difference between them is attributable to the medium effects (harmonic absorption and detuning from the HHG phase matching) that were not taken into account in this theory.

Although this four-step model provides reasonable estimates for the ratio of the enhanced harmonic intensity to the averaged intensity of neighboring harmonics, the authors of Ref. [113] point out that the suppression of harmonics preceding the resonant one remains a puzzle for the theoretical model [111]. Frolov et al. [113] showed in their research that enhancements of single harmonics with energies near the energies of autoionizing states in atoms or atomic ions, as well as the aforementioned suppression of the preceding harmonics, may be interpreted (at least for those harmonics in the region of the classical plateau cut-offs for a given laser frequency and intensity) in terms of the usual three-step scenario of HHG [27], without any additional assumptions or extensions. Notably, they successfully reproduced the main features observed in experiments on HHG from the plasmas produced by the laser ablation of solid Cr and Mn targets. For both 800- and 400-nm laser wavelengths, these features are due to ionic structure effects on the radiative recombination cross sections of Cr^{2+} and Mn^{2+} ions (or, equivalently, on the photoionization cross sections of Cr^{+} and Mn^{+} ions). These effects were predicted by the factorization formula [115] for the HHG rates.

The experimental measurements of these rates serve to complement the measurements of Cooper minima in HHG from neutral atoms [116, 117]. In contrast to manifestations of the Cooper minima in HHG rates, however, which have a predominantly single-electron origin, plasma HHG results can be regarded as the first experimental evidence of genuine multielectron atomic dynamics. Since this dynamics cannot, in principle, be described by the commonly applied single-electron approximation to solution of the time-dependent Schrödinger equation for HHG, the search for atomic targets permitting enhanced harmonic generation in the XUV range should stimulate accurate multielectron calculations of the photoionization cross sections from inner and outer electron shells of complex atoms and ions in order to provide an accurate description of the strongly resonant transitions that underlie the enhanced yield of particular high-order harmonics.

It was found by Milošević [112] that the laser intensity dependence of the intensity and phase of the single harmonic generated in the resonant HHG from plasma ablation differs from that of the standard plateau and near-cutoff higher harmonics. The resonant harmonic intensity increases continuously (i.e., without rapid oscillations) with an increase in the laser intensity, while the resonant harmonic phase remains almost constant. Such unusual behavior of the harmonic phase requires a detailed experimental investigation.

Subfemtosecond light pulses can be obtained by superposing several high-order harmonics. In the context of the recent first attosecond pulse train reconstruction of high-order harmonics from laser ablation plasma [62], the results of Ref. [112] are even more important. It was found that the temporal profile of a group of odd harmonics, which encompasses the resonant harmonic, shows up in the form of a broad peak in each laser-field half-cycle. This is an advantage in comparison with the usual plateau and cut-off harmonics, where two such peaks are generated every half-cycle, which requires the appropriate experimental technique (i.e., such focusing that the collective effects due to the macroscopic propagation select only one emission peak). Taking into account the smooth dependence of the harmonic intensity on the laser intensity, and that it is not necessary to manipulate with long and short orbits of an accelerated electron via appropriate focusing, one can expect that resonant HHG has bright prospects for applications in attoscience [118, 119].

HHG in the presence of a strong resonance was analyzed in paper [114]. To reveal the HHG mechanism, a time–frequency analysis of the intensity and phase was made. It was found that the presence of a resonance gives rise to a clear signature in the HHG spectrum, irrespective of the pulse length. The time–frequency analysis supported Strelkov's four-step model, according to which the recombination process consists of two steps: capture of the returning electron into the resonance, and subsequent radiative transition to the ground state. While the present one-dimensional calculation favors capture from the long trajectory of an accelerated electron, one can expect that a full three-dimensional calculation will show a similar mechanism, but with higher weight given to the short trajectory of this electron. By nature of this process, the emitted harmonic radiation is phase-locked with the usual harmonic emission from the short and long electron trajectories. For long-lived resonances, the interference occurs between the populations caused by re-collisions in different half cycles. This leads to new possibilities for XUV pulse shaping on the subfemtosecond time scale.

In Ref. [49], simulations of resonant HHG were performed by means of a multiconfigurational time-dependent Hartree–Fock approach for 3D fullerene-like systems, and the influence of the C_{60} surface plasmon resonance on the harmonic generation efficiency in the range of 60 nm ($E \sim 20$ eV) was analyzed. Those results showed the ways for resonant HHG optimization and, most important, attosecond pulse train generation. The MCTDHF calculations of HHG from C_{60} clusters proved to be in good qualitative agreement with the experimental data reported in previous studies of harmonic generation in fullerene-containing laser plumes. The broadness of the SPR in C_{60} allows the direct stimulated radiative transition from the continuum to the ground state without the additional need of radiationless transition, thus making possible competing enhancement of

neighboring harmonics, which is useful for attosecond pulse train generation.

In general, multielectron SPR of C_{60} is a generalization to two-electron autoionizing states in atoms and simple molecules. However, the extreme width of the plasmon resonance permits direct recombination, whereas for occupying autoionizing states the radiationless transition to these states should happen first. Usage of a strongly ionized medium with isolated delocalized electrons as a target for resonant HHG can be favorable for the extension of such attosecond pulse trains towards the water-window spectral region.

Research work [53] was devoted to an explanation of the observed phenomenon of resonant enhancement of a single harmonic in indium-ablated plasma without enhancement of neighboring ones. It can also be used to select the most promising targets for resonant HHG and to increase its efficiency by controling the pump radiation parameters. All computations by Redkin et al. [53] were performed using the time-dependent density functional theory (TDDFT) [120] with the aid of OCTOPUS real-space real-time code [121, 122], which is a software package for performing Kohn–Sham TDDFT calculations. A detailed description of the TDDFT formalism can be found in lecture [123]. The results of TDDFT calculations of the HHG in indium-ablated were found to be in good qualitative correlation with experimental data [25]. This allowed proof of the possibility of direct resonant recombination for HHG on the basis of calculations covering artificially chirped pulses. The peculiarities of this approach were also discussed and compared with existing theories of resonant harmonic enhancement.

As a general conclusion, in any time-dependent HHG calculations, which support the presence of strongly excited states, a resonant HHG should be observed if resonant conditions are met at the moment of recombination. The states themselves can be artificially introduced for single-electron models [117] or can follow naturally from the potential well structure in multielectronic calculations. Examples of such approaches are presented in the sections that follow.

4.3 Two-color pump resonance-induced enhancement of odd and even harmonics from a tin plasma

Among the few laser-produced plasmas demonstrating enhanced higher harmonics, tin represents an interesting sample of single-harmonic generation, when strong radiative transitions in singly and doubly charged ions can considerably influence this process, depending on the experimental conditions (wavelength of driving radiation, laser pulse chirp, single- or two-color pump, spectral width of driving radiation, pulse duration, etc.), which was confirmed during experimental and theoretical studies of HHG in an Sn-ablated plasma [36, 43, 111, 124]. In the meantime, a further search for superior properties of this plasma, together with consideration of the role of different plasma species (neutrals, singly and doubly charged ions) in the optimization of a harmonic generation efficiency, can improve our understanding of the role of various ion transitions in the efficiency of this nonlinear optical process. The application of high pulse repetition rate lasers generating broadband ultrashort pulses can also enhance the output power of generating resonant harmonics from a tin plasma.

Below, we discuss theoretical studies of the photoabsorption spectra of different ions in tin plasma [69] and analyze the calculations of the harmonic output for odd and even harmonics under variable experimental conditions, based on the approach developed by Strelkov [111].

From the published data on Sn II radiative transitions in the studied spectral region [125], one can find that the observed enhancement of the 16th harmonic ($E = 25.43$ eV) and the 17th harmonic ($E = 27.02$ eV) of chirp-free 780-nm laser radiation can be attributed to the transitions $4d^{10}5s^25p\,{}^2P_{3/2} \rightarrow 4d^95s^25p^2$. The frequencies of these transitions, some of which possess reasonably large oscillator strengths, lie in the photon energy range from 24.9 to 27.3 eV. One can also attribute the observed enhancement of the 15th harmonic (generated by the negatively chirped pulse) to its approach towards the range of the $4d^{10}5s^25p\,{}^2P_{3/2} \rightarrow 4d^95s^25p^2$ transitions in the Sn II ion. However, Sn II radiative transitions cannot adequately explain the enhancement of the 17th harmonic, when the pulse chirp variations cause a blue shift of radiation frequency and its subsequent generation at a wavelength of 45.1 nm ($E = 27.49$ eV). Therefore, one has to also consider the Sn III ions as a potential source of enhancement of this harmonic.

In order to simulate resonant HHG enhancement in Sn II and Sn III ions, one has to calculate the characteristics of the autoionizing (AI) states in these ions. Duffy et al. [125] recorded $4d \rightarrow 5p$ photoabsorption spectra of Sn II and Sn III ions in the 23–33 eV range. Transitions from the $4d^{10}5s^25p$ ground state of Sn II and from the $4d^{10}5s^2$ ground and $4d^{10}5s5p$ excited states of Sn III were detected and successfully identified with the aid of multiconfigurational Hartree–Fock calculations. These calculations were repeated in the study under discussion [69] to replicate these optical spectra and provide estimates of the autoionizing widths for the dominant transitions.

For the Sn II ($I_p = 14.63$ eV) spectrum configuration, the interaction calculations were performed in the self-consistent Russell–Saunders coupling scheme with the HXR mode (Hartree plus exchange plus relativistic corrections) of the Cowan code [126] for radiative transitions between the ion states $4d^{10}5s^25p \rightarrow 4d^95s^25p$, np, mf ($5 \leqslant n \leqslant 13$, $4 \leqslant m \leqslant 13$). The Slater parameters F^k, G^k and the configuration interaction parameter R^k were fixed at 85% of the *ab initio* values, while the spin–orbit parameter was left unchanged. Good agreement was achieved between the calculated transition energies and strength values obtained in the previous work [125], with maximum discrepancies of 0.12 eV and 0.09, respectively, which may be attributed to the increased basis set and scaling factors in the discussed study. Calculations were performed to determine the autoionizing decay widths of the excited $4d^{-1}$ states, which are allowed to decay by the following processes:

$$4d^95s^25p\,np, mf \rightarrow 4d^{10}5s^2 + \varepsilon l \qquad (l = 0, 2, 4)\,, \qquad (12)$$

$$\rightarrow 4d^{10}5s5p + \varepsilon' l \qquad (l = 1, 3)\,, \qquad (13)$$

$$\rightarrow 4d^{10}5p^2 + \varepsilon'' l \qquad (l = 2)\,. \qquad (14)$$

Here, l is the azimuthal (orbital) quantum number.

The values of ε, ε', and ε'' are the differences in the configuration-average energies of the excited $4d^{-1}$ configuration and each final Sn III ion configuration. Synthetic spectra were constructed by assuming a Lorentzian line profile:

$$\sigma(E) = \frac{109.7 f_k \Gamma_k}{2\pi\left[(E_k - E)^2 + \Gamma_k^2/4\right]}\,,$$

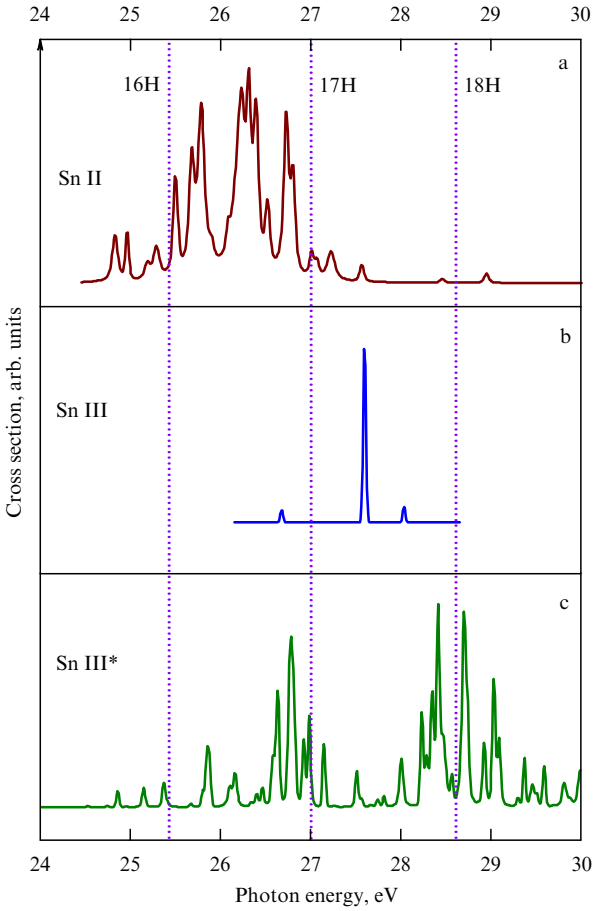

Figure 6. The photoabsorption cross section spectra of Sn II $4d^{10}5s^25p \rightarrow 4d^95s^25p^2$ (a), Sn III $4d^{10}5s^2 \rightarrow 4d^95s^25p$ (b), and Sn III* $4d^{10}5s5p \rightarrow 4d^95s5p^2$ (c) excited states convolved with a Gaussian instrumental function 30 meV in width. Dashed lines show 780-nm radiation harmonic frequencies [69].

where E_k and Γ_k are the energy and autoionization decay width of the radiative transition in eV, f_k is the oscillator strength, and k is the number of state. The synthetic spectrum was then convolved with a Gaussian instrumental function of width 0.030 eV; it is presented in Fig. 6.

For Sn III spectra, calculations were performed in a *jj*-coupling scheme for transitions from both the ground $4d^{10}5s^2$ and the excited $4d^{10}5s5p$ electron configurations, which has a configuration-average energy of 6.87 eV. In these calculations, the Slater integrals were scaled to 80%, except the spin–orbit integral which was left unchanged. The $4d^95s^25p$ electron configuration (the configuration-average energy of 26.91 eV) does not autoionize, because it lies below the ionization limit of an Sn IV ion (30.50 eV [127]). The excited $4d^95s5p^2$ configuration has a configuration-average energy of 35.22 eV and, therefore, once populated $4d^{10}5s5p$ excited state can autoionize through the following processes

$$4d^95s5p^2 \rightarrow 4d^{10}5s + \varepsilon l \quad (l = 0, 2, 4)\,, \tag{15}$$

where the values of ε are the differences in the configuration-average energies of the excited $4d^{-1}$ configuration and each final Sn IV ion configuration. The resulting synthetic spectra, which were convolved with a Gaussian instrumental function 0.030 eV in width, are also presented in Fig. 6. The radiative transition characteristics required for resonant HHG simulation are listed in Table 1. The experimentally observed enhancement of the blue-shifted 17th harmonic (at $\lambda = 45.1$ nm) [69] can be attributed to the Sn III transitions $4d^{10}5s^2 \rightarrow 4d^95s^25p$ ($E = 27.6$ eV, $\lambda = 44.92$ nm). It should be noted that autoionizing states are not involved in this transition; thus, this enhancement cannot be explained via the four-step model [111]. The enhancement can be ascribed to better phase-matching conditions near the resonance [2], and/or to the mechanism of single-atom response enhancement. Understanding the origin of this enhancement requires further studies.

Resonant HHG simulation is based on the numerical solution of the 3D time-dependent Schrödinger equation (TDSE) for a model ion in an external laser field. One can rely on a single-electron approximation accounting for the interaction with other electrons and with a nucleus with a model potential, as was done in Refs [111, 114]. This method is applicable, in particular, to the description of the resonances in the Sn II and Sn III ions. The following form of the model potential for the parent ion was utilized (atomic units are used throughout):

$$V(r) = -\frac{Q+1}{\sqrt{a_0^2 + r^2}} + a_1 \exp\left[-\left(\frac{r - a_2}{a_3}\right)^2\right], \tag{16}$$

where Q is the charge state of the generating ion (1 for Sn II, and 2 for Sn III), a_0, a_1, a_2, and a_3 are the fitting parameters, and r is the polar coordinate.

These parameters are chosen to reproduce the properties of certain radiative transitions in Sn II and Sn III* ions. Namely, Sn II undergoes a transition $4d^{10}5s^25p\,^2P_{3/2} \rightarrow 4d^95s^25p^2\,(^1D)\,^2D_{5/2}$ with a frequency ($E = 26.22$ eV) close to the 16th and 17th harmonic frequencies of the 780-nm chirp-free driving radiation and with an oscillator strength essentially exceeding those for the other transitions in this spectral region. Thus, one can neglect the other AI states in this ion and choose the potential parameters to reproduce this AI state energy, the ground state energy, the AI state linewidth, and the oscillator strength of the transition. For a

Table 1. Autoionizing properties of some transitions in tin ions.

Ion	Transition	E_{calc}, eV	gf [1*]	Γ, meV
Sn II	$4d^{10}5s^25p\,^2P_{3/2} \rightarrow 4d^95s^25p^2\,^2D_{5/2}$	26.22 [2*]	1.43	160.0
Sn III	$4d^{10}5s^2\,^1S_0 \rightarrow 4d^95s^25p\,^1P_1$	27.6 [3*]	0.87	—
Sn III*	$4d^{10}5s5p(1/2, 3/2)_2 \rightarrow 4d^95s5p^2(5/2, 1/2)_3$ [4*]	28.48 [5*]	0.84	47.20

[1*] The gf quantity is the product of the oscillator strength f of a transition and the statistical weight g of the lower energy level.
[2*, 5*] Calculated energies were shifted by 0.46 eV and −0.65 eV, respectively.
[3*] Calculated energies were shifted by 0.16 eV.
[4*] The *jj*-coupling is denoted by $(J_{core}, J_{n\ell})_J$, where the subscript J refers to the total angular momentum of the level.

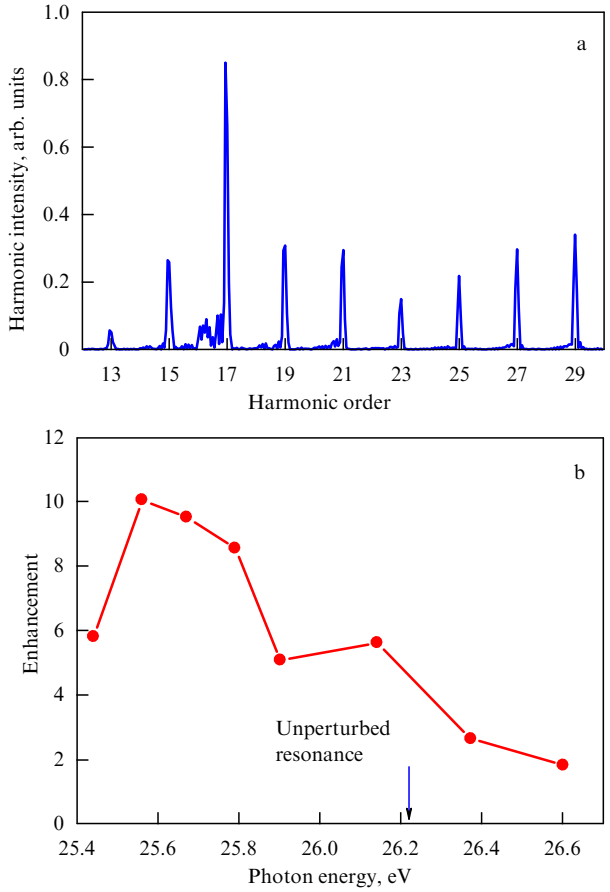

Figure 7. (a) Harmonic spectrum calculated for Sn II. The laser intensity is 10^{15} W cm^{-2}. (b) The calculated resonant 17th harmonic enhancement as a function of the harmonic photon energy. The arrow shows the transition frequency in the absence of the laser field [69].

doubly ionized Sn III* ion, the transition with a frequency of 28.48 eV has the greatest oscillator strength in this spectral region. So, simulating HHG with Sn III* ions, one can choose the model potential parameters to reproduce the properties of this transition. The method of the TDSE solution was described in Ref. [128]. The spectrum of the microscopic response calculated for the Sn II ion is presented in Fig. 7a. One can see the pronounced enhancement of the 17th harmonic, in agreement with the experimental results reported in Ref. [69].

To study the frequency range in which the harmonic is enhanced, the HHG from Sn II ions was calculated using slightly different fundamental frequencies. The frequency dependence of the harmonic enhancement is presented in Fig. 7b. It is readily seen that maximum enhancement is achieved for a frequency that differs from the transition frequency in the absence of the laser radiation, thus conforming to experimental results [43]. This difference can be attributed to the Stark shift of the AI and ground states in the laser field. The width of the spectral range where the harmonic is enhanced measures about 0.7 eV (FWHM). This is higher than the AI state width calculated in the absence of the laser field (0.160 eV, see Table 1) and used in this model. This peculiarity may be explained by the broadening of the AI state due to its photoionization by the laser field.

4.4 Calculations of single harmonic generation from Mn plasma

In this section, we present the results of numerical simulations of high-harmonic generation in manganese plasma within a 1D model [129]. It was assumed that the main contribution to the resonance peak in the spectrum observed in experiment [129] comes from Mn^+ ions. Notice that the ionization potential of Mn^{2+} ions (33.7 eV) is more than twice as high as that of Mn^+ ions (15.6 eV). The time-dependent Schrödinger equation was solved by means of the split-operator method [130]. The Mn^+ target was modeled using a potential supporting a metastable state by a potential barrier [111, 114]. The shape of the potential is as follows (Fig. 8a):

$$V(x) = -a + \frac{a}{1+\exp\left[(x+b)/c\right]} + \frac{a}{1+\exp\left[(-x+b)/c\right]} + \frac{d/(e+x^2)}{1+\exp\left[(x+b)/c\right]} + \frac{d/(e+x^2)}{1+\exp\left[(-x+b)/c\right]}, \quad (17)$$

where a, b, c, d, and e are parameters chosen to be 1.672, 1.16, 0.216, 8.95, and 0.63, respectively, so that the width of the

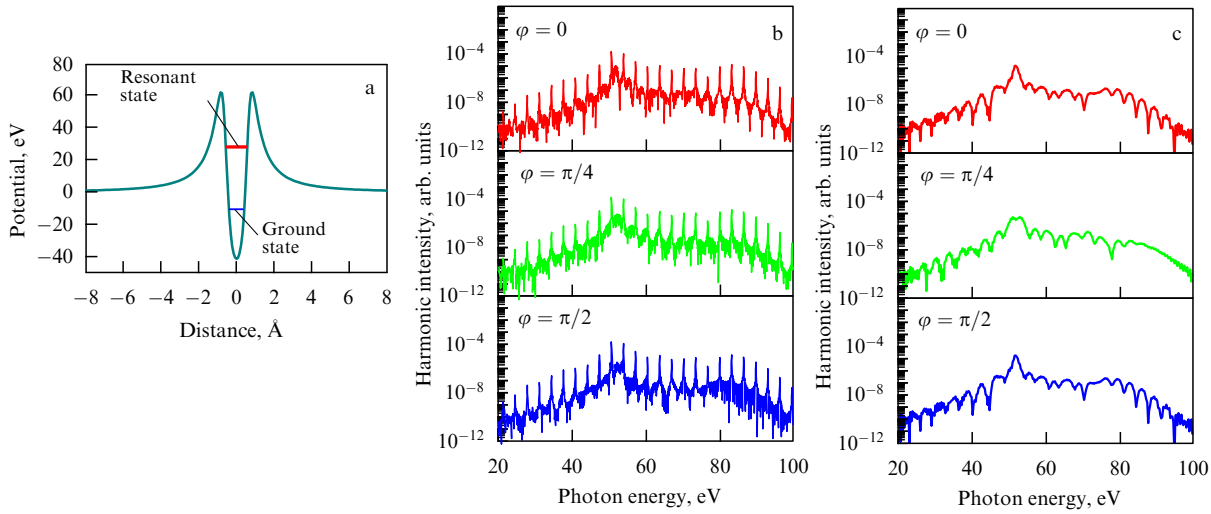

Figure 8. (a) Potential used for numerical simulations. (b, c) Calculated HHG spectra using (b) a long (40 fs) pulse, and (c) few-cycle pulses at different values of the CEP ($\varphi = 0$, $\pi/4$, and $\pi/2$) [129].

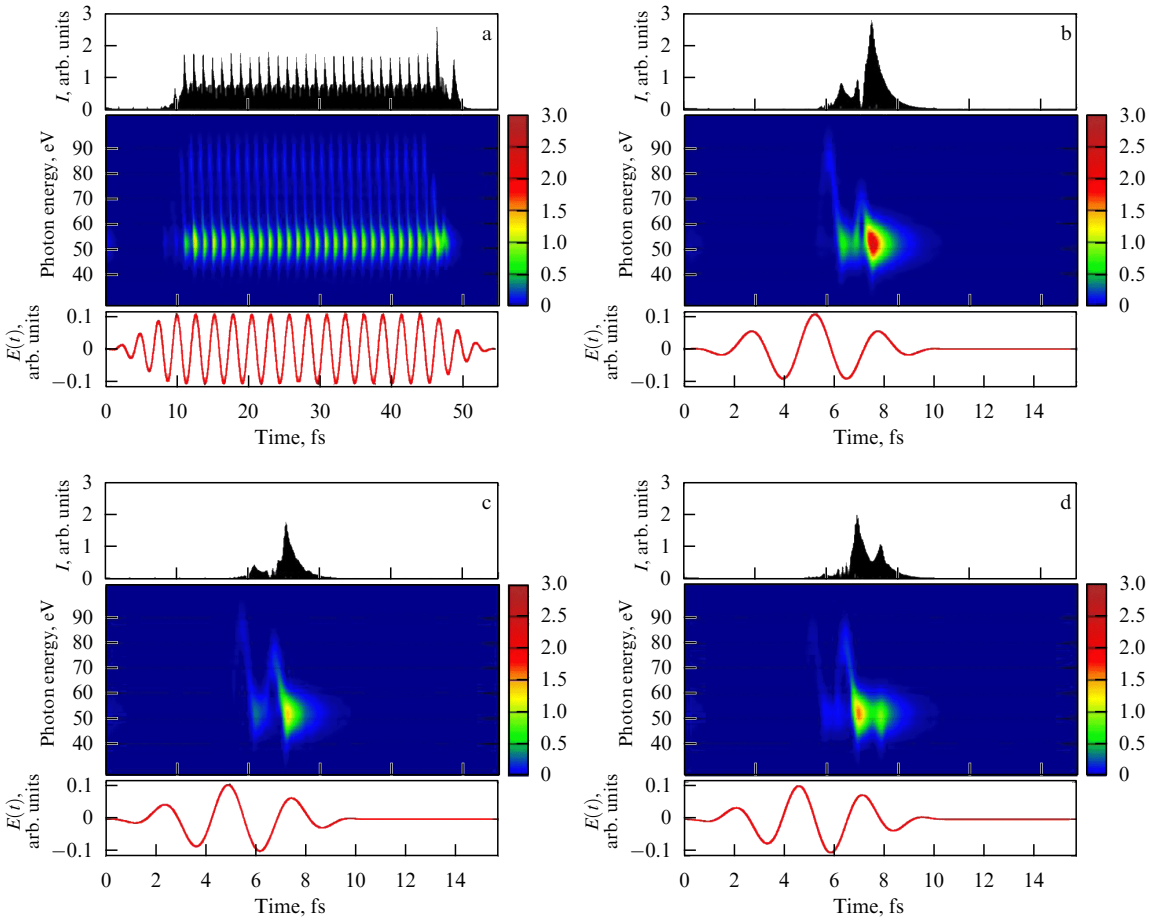

Figure 9. (Color online.) Calculated results for HHG driven by (a) a long (40 fs) pulse with CEP $\varphi = \pi/4$, and (b–d) few-cycle pulses with CEPs of (b) $\varphi = 0$, (c) $\varphi = \pi/4$, and (d) $\varphi = \pi/2$. The top panels show the HHG temporal intensity profile obtained as the square of the time-dependent dipole acceleration after high-pass filtering above 32.7 eV. The middle panels show the time–frequency diagrams. The red curves in the bottom panels show the time dependence of the electric field of the driving laser pulse [129].

resonance and the energy gap between the ground and the resonant states resembles the experimental data [131]. The metastable state in this model potential is located 51.8 eV above the ground state. The laser field is approximated by $E(t) = E_0 f(t) \cos(\omega_0 t + \varphi)$, where $f(t)$ is the pulse envelope, φ denotes the carrier envelope phase (CEP), and ω_0 is the laser frequency corresponding to the central wavelength $\lambda = 760$ nm. The laser intensity is $I_0 = 4 \times 10^{14}$ W cm^{-2}. A CEP of $\varphi = 0$ means that the maximum of the envelope corresponds to a maximum of $\sin(\omega_0 t)$.

HHG spectra were calculated for pulse shapes with different lengths and for different values of φ (Fig. 8b, c). A $\sin^2$ envelope with a total length of 4 full cycles was used to model the 3.5-fs laser pulse, while an envelope with 4 cycles $\sin^2$ switch-on/off, 13 cycles of constant intensity, and, consequently, 21 cycles total duration was utilized to model the 40-fs case. The long pulse led to an HHG spectrum that showed well-defined peaks at the odd harmonic orders and exhibited a weak dependence on the CEP (Fig. 8b). Figure 8c plots the dependence of the harmonic spectrum on the CEP for short, few-cycle pulse. In all cases, the resonance dominated the spectrum. The most intense emission occurred around 51 eV, where the metastable state is located. Although some difference between resonant harmonic spectra at $\varphi = 0$, $\pi/4$, and $\pi/2$ is found, we note that the CEP dependence is strongest for the spectrum outside the region of the resonance. For random CEP, the substructure of the spectrum will average out, as confirmed by numerical averaging over 20 values of the CEP in the range from 0 to π. The resonance peak itself depends less on the CEP. The case of $\varphi = \pi/4$ appears to be special, since a dip due to trajectory interference seems to coincide with the resonance peak.

In order to investigate the temporal characteristics of the harmonic emission in numerical simulations, a Gabor transformation was performed [132]:

$$G(\omega, t) = (2\pi\sigma^2)^{-1/2} \int \mathrm{d}\tau\, a(\tau) \exp(\mathrm{i}\omega\tau) \exp\left[-\frac{(t-\tau)^2}{2\sigma^2}\right], \tag{18}$$

where $a(\tau)$ is the dipole acceleration deduced from the simulation, and σ is the parameter equal to $1/(3\omega_0)$. The modulus squared, $|G(\omega, t)|^2$, defines the time–frequency distribution. The temporal intensity profile of the XUV emission is calculated as the square of the time-dependent dipole acceleration after filtering out the photon energies below 1.2 atomic units (corresponding to 32.7 eV). In fact, the emission profile is not much affected by the filtering, since the spectrum is strongly dominated by the resonance. The calculated results are given in Fig. 9. Comparing the short- and long-pulse regimes, one can notice that, whereas in

Fig. 9b–d resonance emission occurs at the end of the few-cycle pulse, Fig. 9a shows that the resonance state is repopulated and decays each half cycle of the multicycle pulse.

For most CEPs, the emitted radiation can be viewed as an isolated sub-fs XUV pulse if the pulse length is defined, in the usual way, as the full width at half maximum. This main emission burst is either preceded or followed by a small side peak. Similar emission profiles were found for three values of the CEP (0, $\pi/4$, and $\pi/2$, Fig. 9b–d). The time of maximum emission varies in a range of less than 1 fs with CEP. These calculations show that one can usually get subfemtosecond XUV pulses, or at least $\sim$ 1-femtosecond XUV pulses, for different values of the CEP. This is in sharp contrast with the usual strong CEP dependence of isolated attosecond pulse generation [133–135], suggesting that resonance-induced HHG driven by few-cycle pulses provides a route to isolated XUV attosecond pulse generation with reduced requirements for CEP stabilization.

5. Harmonic generation of picosecond Nd:YAG laser radiation in ablation-produced plasmas

As was already pointed out, the advantages of HHG in a plasma plume could largely be realized employing the low-excited and weakly ionized plasma, because in that case the limiting processes governing the dynamics of the laser frequency conversion would play a minor role [4, 136, 137]. A search for the best experimental conditions, such as the pulse duration of a driving laser field, for efficient HHG in different spectral ranges is a way to further enhance harmonic yield.

Almost all previous plasma HHG studies were carried out with femtosecond pulses. The spectral range of those experiments was restricted at the longer-wavelength side to $\sim$ 80 nm, which was determined by the registration properties of the commonly used detectors of harmonic spectra (microchannel plates). A limited number of studies into plasma HHG were performed in the spectral region above this wavelength. A search for resonance enhancement of a single harmonic under these conditions can be justified by the presence of strong ion and neutral transitions in the longer-wavelength vacuum ultraviolet range (80–200 nm). Next, the application of longer pulses could avoid the impeding processes restricting the efficiency of harmonic generation in this region. There are two main limiting processes which can decrease the conversion efficiency in the ionic medium. The first one is an excess of free-electron concentration caused by overexcitation of the target surface. The appearance of a considerable number of free electrons is a result of the ionization of both neutral atoms and singly charged particles. This results in self-defocusing of the propagating probe pulse. The second process is directly related to the first one. The phase matching conditions of the driving and harmonic waves, which are maintained for a moderate number of free electrons appearing during ionization of neutrals in the ablation process, break up due to an increase in free electron concentration. This increase occurs abruptly once the fluence of the heating pulse reaches the threshold level, when the overexcitation of targets leads to the appearance of doubly and multiply charged particles. Furthermore, the use of longer pulses can also increase the fluence of harmonic emission at comparable HHG conversion efficiencies from picosecond and femtosecond sources due to the higher pulse energies available in the former case.

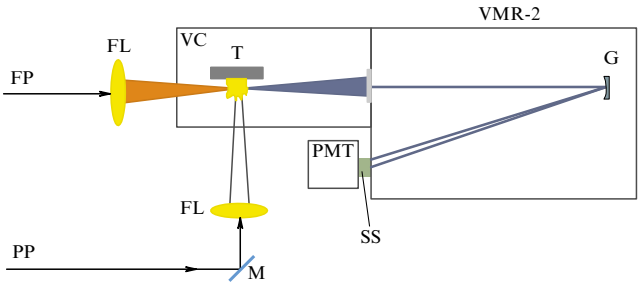

Figure 10. Experimental setup for studying HHG in a laser plasma using picosecond pulses: FP, fundamental probe picosecond pulse; PP, heating picosecond pulse; M, mirror; FL, focusing lenses; VC, vacuum chamber; T, target; VMR-2, vacuum monochromator; G, grating; SS, sodium salicylate, and PMT, photomultiplier tube [138].

Recent studies have shown the attractiveness of the application of long laser pulses for third-order harmonic generation from laser plasmas [61, 68, 74]. Below, we present an analysis of the higher-order harmonics generated in various plasmas by utilizing 1064-nm, 38-ps pulses [138]. The goal of those studies was to search for the conditions of generation of energetic coherent picosecond pulses in the range of 80–220 nm employing diverse metal-ablated plasma plumes.

A passive mode-locked Nd:YAG laser (1064-nm, 1.5-Hz pulse repetition rate) generated a 38-ps pulse. Two-stage amplification of the single pulse was followed by the splitting of this radiation into two parts, one (heating pulse) with an energy of 5 mJ, which was used for plasma formation on the target surface, and the other (probe pulse) with an energy of up to 28 mJ, which was used after some delay for frequency conversion in various plasma plumes (Fig. 10). The heating pulse was focused with the aid of a 300-mm focal length lens inside a vacuum chamber containing the targets. A variety of metal materials (copper, chromium, zinc, niobium, silver, indium, molybdenum, titanium, tin, lead, tantalum, manganese, tungsten, gold, boron, and aluminum) were tapped as the targets for laser-induced plasma formation. The plasma cloud sizes were in the range of 0.5 mm. The heating pulse intensity on the target surface run to $\sim 10^{11}$ W cm^{-2}. The diameter of the single-mode probe beam measured 4 mm. This beam was focused inside the plasma plume with the aid of a 150-mm focal length lens. The probe beam propagated at a distance of 100–150 μm from the surface of the target. The intensity of the probe pulse at the focus reached 4×10^{13} W cm^{-2}. The focal spot resided inside the plasma plume. The time delay between the heating and probe pulses was maintained at 25 ns, which was optimal for efficient harmonic generation in most of the metal-containing plasmas. The harmonic radiation was analyzed with a vacuum monochromator.

Analysis of the evolution of the optical spectra of laser plasma provides important information about the plasma parameters and can be used for multiple applications. Notably, time-resolved laser-induced plasma spectrometry in studies of high-harmonic generation in gold, silver, manganese, and vanadium plasmas [42] allowed the identification of emissions from native species and optimization of conditions when the plasma mostly consisted of excited neutrals and singly charged ions. It should be noted that

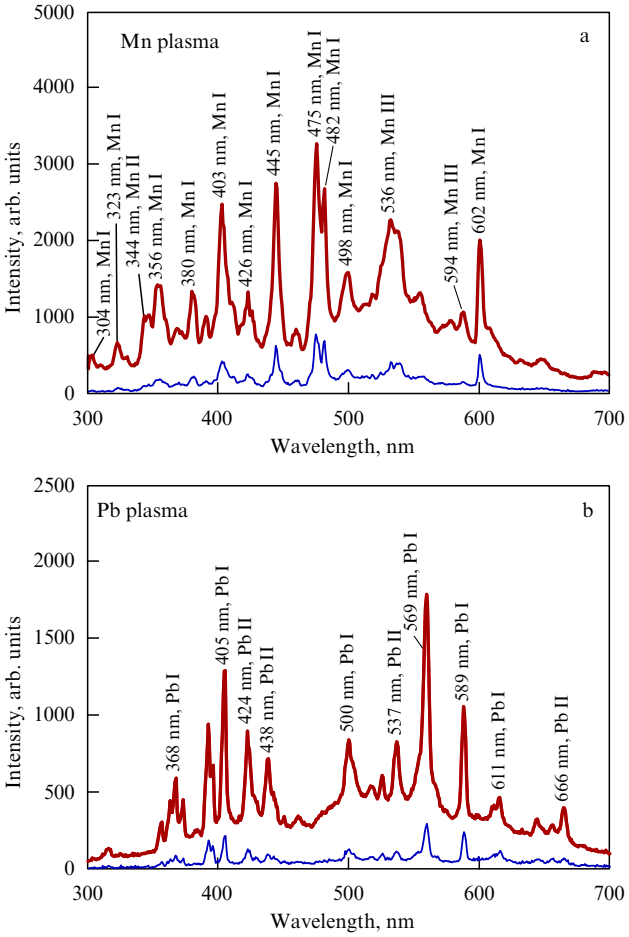

Figure 11. Plasma emission spectra from (a) Mn and (b) Pb targets under weak (thin lines, $I = 8 \times 10^{10}$ W cm^{-2}) and strong (thick lines, $I = 2 \times 10^{11}$ W cm^{-2}) excitations of target surfaces [138].

most plasma HHG studies were carried out applying time-integrated methods of plasma emission analysis, so it was impossible to define exactly what plasma conditions existed during the propagation of the femtosecond pulse through the plume. Below, we discuss a time-integrated analysis of spectral studies of plasma emission from various metal targets involved in harmonic generation during propagation of picosecond laser radiation through plasma. Those studies were aimed at defining the optimal plasma conditions for efficient HHG from laser plumes and showed that, while for most plasma plumes overexcitation during laser ablation leads to a drastic decrease in harmonic generation efficiency, in some cases one can achieve the conditions for extension of the harmonic cutoff with picosecond probe pulses.

Spectral studies of atomic and ion emissions from laser-produced plasmas have been carried out in the visible and near-ultraviolet (UV) ranges (300–700 nm). This spectral region was chosen due to the existence of multiple ion and atomic radiative transitions in the plasma species studied. To perform the ablation, a 1064-nm, 38-ps pulse from an Nd:YAG laser was focused at different intensities onto a metal target in a vacuum chamber. The spectral characteristics of the laser plasma in the visible and UV ranges were analyzed with a fiber spectrometer (HR4000).

The spectra of plasma emission from Mn- and Pb-ablated plasmas are presented in Fig. 11. The spectral lines mostly originated from the excited states of neutral and singly charged ions, when the impeding influence of free electrons on the high-order nonlinear optical processes in the laser plasmas was insignificant. An increase in heating pulse intensity on the target surfaces above 10^{11} W cm^{-2} led to both the growth of emission intensity for neutral and singly charged ion species and the appearance of emission lines from the higher-charged particles. The appearance of doubly and triply charged ions and a large number of free electrons was immediately followed by a considerable decrease in HHG conversion efficiency from almost all the plasma samples. The variations of the plasma spectra in that case are presented in Fig. 11, where one can examine the changes in the intensity of plasma emission from the Pb and Mn targets. The thin and thick curves correspond to weak and strong excitations, respectively. This figure clearly shows an increase in the intensities of Mn III and Pb II lines, which correlates to an increase in the concentration of multiply charged ions in the plasma plume and, correspondingly, the concentration of free electrons.

In Ref. [138], the restricting features of harmonic generation dynamics during overexcitation of the targets were observed in most of the plasma plumes analyzed. The increase in heating pulse intensity from 1×10^{11} to 3×10^{11} W cm^{-2} in HHG experiments with these targets led to the appearance of strong plasma emission. Under these excitation conditions, the harmonic emission from various plasmas overlapped with plasma emission. The intensity of the generated harmonics became considerably weaker than at 1×10^{11}-W cm^{-2} excitation. In most of the plasmas, this overexcitation led to a complete disappearance of harmonic emission. The variations of HHG efficiency with the growth in heating pulse intensity are depicted in Fig. 12. In particular, the 11th harmonic generated from the Pb plasma started to decrease its intensity with the growth of the heating pulse energy above 3 mJ (Fig. 12a), which corresponded to a pulse intensity of 1×10^{11} W cm^{-2}. In another case, an intensity decrease in the 5th, 7th, and 9th harmonics generated in Mn plasma was observed at pulse energies above 1.5 mJ (Fig. 12b).

The reason for the decrease in harmonic conversion efficiency is related to overexcitation of the target, which led to the appearance of an abundance of free electrons in the plasma plume. As noted above, the latter causes a phase mismatch between the waves of the driving field and the harmonics. This effect is especially important for the lower-order harmonics. One may call attention to the fact that a decrease in harmonic efficiency with over-excitation of plasma has been reported for higher-order harmonics as well [139], although this decrease in converted XUV radiation was less abrupt than that observed in the studies discussed.

The characteristic pattern of almost all the harmonic spectra from metal plasmas was a featureless steep decrease in conversion efficiency for the lowest orders, which was followed by a gradual intensity decrease in higher harmonics (a so-called plateau-like shape) up to the limit of the registration range of the monochromator (50 nm, 21st harmonic). Figure 13a shows the characteristic HHG spectra obtained from Cr, Cu, and Ti plasmas. Most of these plasmas exhibited comparable nonlinear optical properties from the point of view of HHG conversion efficiency.

Measurements of the absolute values of the conversion efficiencies of the harmonics generated in the plasmas were carried out using the following procedure. In the first step, the 4th harmonic signal was measured by a 'monochromator + sodium salicylate + photomultiplier tube' detection system

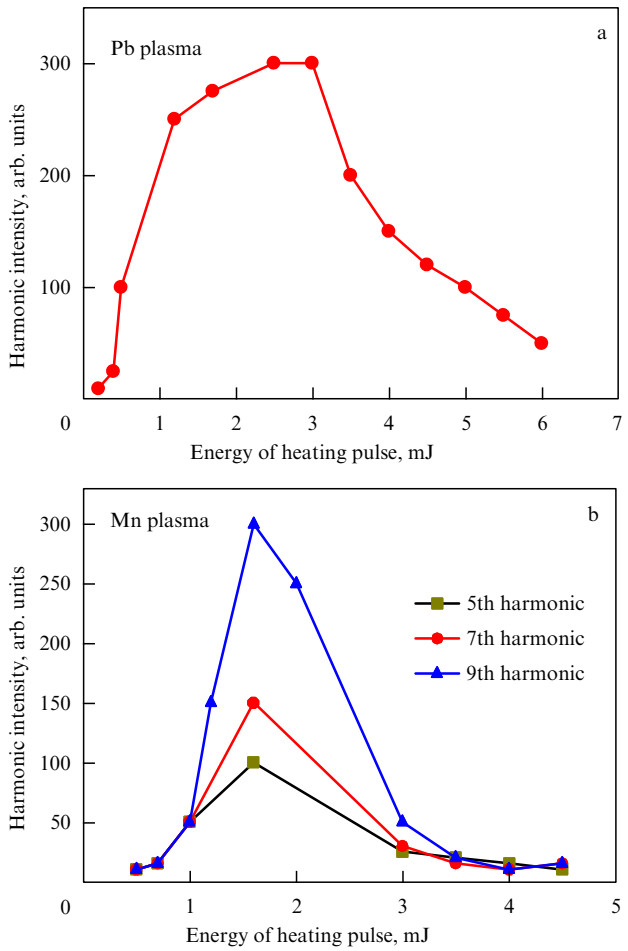

Figure 12. Dependences of harmonic intensity at different heating pulse energies for (a) the 11th harmonic generated from Pb plasma, and (b) the 5th, 7th, and 9th harmonics generated from Mn plasma [138].

using the known energy of the 4th harmonic of 1064-nm radiation generated in nonlinear crystals. This allowed calibration of the monochromator against a wavelength of 266 nm. Since the quantum yield of sodium salicylate is equal in a broad spectral range between 40 and 350 nm, calibration of the registration system against 266-nm line allowed the calculation of the conversion efficiency for the higher harmonics. The monochromator was used for the observation of the harmonics between 300 and 50 nm. The conversion efficiency of the plateau harmonics (15th–21st orders) was measured to lie in the range of $10^{-6}-10^{-5}$. Table 2 summarizes the conversion efficiencies for different harmonics in some metal-containing plasma plumes.

While most of the plasmas demonstrated similar properties, some of them showed an unusual spectral distribution of harmonics. In particular, the generation of harmonics was restricted in some cases to the 9th–15th orders. Among these species were the Al, B, and Mo plasma plumes (Fig. 13b). A few other plasmas showed even more interesting spectra, where one could distinguish the enhancement of some harmonics with regard to the lower-order ones. These were the In and Nb plasma plumes, which exhibited an enhancement of 11th harmonics, compared with lower harmonic orders (Fig. 13c). Such dependences resemble those observed in previous plasma HHG experiments utilizing 800-nm pulses a few dozen femtoseconds in duration for In, Mn, Cr, Sn and other plasmas [2, 4]. The commonly accepted explanation of these enhancements has a bearing on the closeness of the wavelengths of specific order harmonics to the ion resonance transitions in these media. Below, we discuss this peculiarity in more details.

The observation of resonance enhancement in both femtosecond and picosecond probe pulses is related to the coincidence of harmonic and ion transition wavelengths. In the case of femtosecond pulses, this opportunity has more chance of being realized due to the broader bandwidths of the harmonic radiation. However, the conditions of resonance enhancement could be realized in picosecond pulses as well, since some of the resonances in Nb and In ions occasionally coincide with the wavelength of the 11th harmonic. These observations were repeated several times in analogous studies of the same plasmas, while none of the other plasma plumes demonstrated these features.

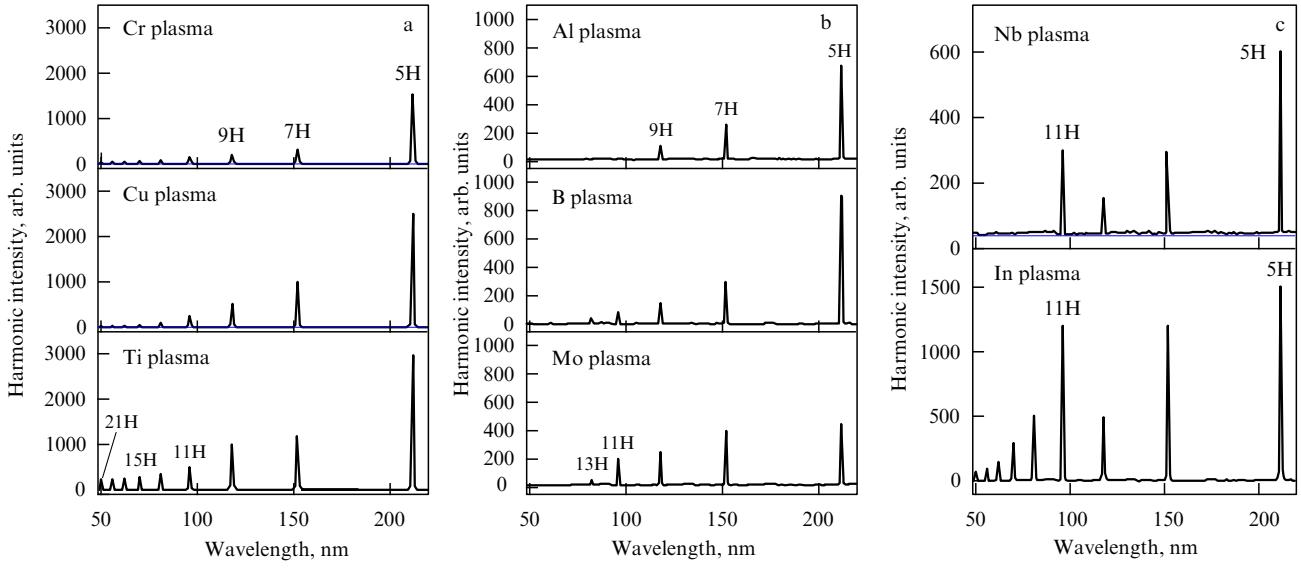

Figure 13. (a) High-order harmonic spectra from Cr, Cu, and Ti plasma plumes. (b) Harmonic spectra from Al, B, and Mo plasmas producing only low-order harmonics. (c) Harmonic spectra from Nb and In plasmas demonstrating the enhancement of the 11th harmonic with regard to the lower-order ones [138].

Table 2. Harmonic conversion efficiencies ($\times 10^{-6}$) from various plasma plumes produced on metal surfaces in the case of converting 38-ps probe laser pulses.

Harmonic order	Wavelength, nm	Sn	Zn	Mn	Ti	Cu	W	Au	B	Ta	Ag	Cr	Mo	Al
5	213	100	80	80	70	46	46	40	40	26	20	20	4.2	6
7	152	66	66	20	20	33	40	33	13	10	16	7.1	3.8	2.59
9	118	66	53	10	12	15	38	26	3	3	10	3.8	2.5	1.33
11	97	53	40	6.6	6.6	13	33	20	1.3	1.8	6.6	3.8	2.1	
13	82	26	4	2.1	4.6	2.5	7	1.8	1	0.9	2.6	1.3	0.9	
15	71	16	4	1.75	3.3	0.9	5	1.3		0.9	1.3	0.9		
17	63	6	1.7	1.3	2.1	0.9		1.3		0.9	1	0.9		
19	56	6	1.7	1.3	2.1	0.83		0.9		0.75	1	0.9		
21	51	4	1	1.3	2.1	0.75		0.9		0.75	1	0.9		

Pulse propagation effects could not explain these evidences since, in that case, we would have to observe the enhancement of at least a few neighboring harmonics as well. One can note that the resonance enhancement of plasma harmonics in the case of narrowband probe pulses is indeed a rarely observed phenomenon. The application of various plumes showed this enhancement only in the two above-mentioned plasmas, while many more plasmas were reported as suitable for resonance enhancement with femtosecond broadband pulses. Figure 13 emphasizes the peculiarities of the harmonic distribution observed in some plasma plumes. Those observations indicated that the atomic number of the element does not play a significant role in the classification of the harmonic properties in the plasma media. The important parameter here could be a second ionization potential of the species used.

A few properties of the generated harmonics from metal-ablated plasmas have been analyzed in depth. The time delay between heating and probe pulses is crucial for optimization of HHG. The concentration of particles (neutrals and singly charged ions) is insufficiently high at the initial stages of plasma formation and spreading out of the target surface material, since the species possessing velocities in the range of $(2-5) \times 10^5$ cm s^{-1} do not reach the optical axis of propagation of the probe beam (100–150 μm above the target surface). An increase in the time delay above 5 ns allowed the appearance of plasma particles in the path of the converting laser pulse, which led to considerable growth of the HHG conversion efficiency. A further increase in the time delay led to saturation of the HHG and a gradual decrease in the conversion efficiency at longer delays. One can note that there are different optimal time delays for the harmonics generated in Mn and Pb plasmas (20 ns and 90 ns, respectively). These observations can be explained by the different velocities of the ablated particles from the targets, which should reach the area of interaction with the probe pulses at different times. In this connection, the application of a heavier target (Pb, $Z = 82$) should lead to a longer delay before the bulk amount of ablated material starts to interact with the probe laser beam, compared with a lighter target (Mn, $Z = 25$). The ratio between optimal time delays for these plasma samples approximately coincides with the ratio between the atomic masses of those particles, given the equal kinetic energies of ablated particles.

Usually, the plasma lifetime is on the order of a few nanoseconds [140]. However, one should consider as another parameter the time when the maximum concentration of particles emerges above the target surface in the area of propagation of the driving laser pulse. Since the distance from the target to the axis of driving pulse propagation is on the order of 100–150 μm, the time when the main cloud of particles reaches this area is around a few dozen nanoseconds and is defined by the velocity of the particles ($\sim 5 \times 10^3$ m s^{-1} for the target atoms with low Z, and $\sim 2 \times 10^3$ m s^{-1} for the targets with high Z). This time is on the order of 20 or 50 ns. So, the value of the plasma lifetime is invalid once we consider the process which depends only on the time required to spread the plasma particles towards the area where the driving pulse propagates. In particular, plasma harmonic experiments [68] using nanosecond pulses were optimized at a 600-ns delay due to the longer distance (~ 1 mm) from the target to the nanosecond probe pulse. The above estimates allowed concluding that the plasma spreading time, which is more critical than the plasma lifetime, is a crucial parameter for achieving efficient HHG.

Another important parameter of plasma HHG is polarization of the probe radiation. A small departure from linear polarization led to a considerable decrease in the harmonic intensities, which is a typical behavior for high-order harmonics. The application of circularly polarized laser pulses led to a complete disappearance of harmonic emission, as should occur assuming the origin of HHG.

The harmonic intensity also considerably depends on the distance between the optical axis of the driving beam and the target surface. This dependence is caused by the change in plasma concentration above the target surface. The log–log dependence of the harmonic intensity (I_h) on the distance (x) between the optical axis of the driving beam and the target surface for the 7th harmonic generated in manganese-ablated plasma corresponded to $I_h \sim x^{-3.5}$.

Let us recall that the earliest observations of HHG in gases were also reported using a picosecond Nd:YAG laser [141, 142] (as well as an excimer laser at 248 nm [143]). The harmonics from different gases up to the 21st and 33rd orders, converted from 1064-nm laser radiation, were reported at an intensity of 3×10^{13} W cm^{-2}, which led to an enormous growth of interest in this area of nonlinear optics. These studies [138] have demonstrated that the application of metal-ablated plasma as a nonlinear medium can further amend this HHG technique on using picosecond driving pulses, once the metal atoms, ions, and clusters become involved as efficient sources of harmonic generation.

6. Stable generation of higher harmonics of femtosecond laser radiation in laser-produced plasma plumes at 1-kHz pulse repetition rate

Almost all HHG studies of weakly ionized plasma plumes produced during laser ablation of various solid targets were carried out with the aid of 10-Hz pulse repetition rate lasers [4, 5]. To date, only a few studies of HHG from plasmas have been carried out on static targets using 1-kHz class lasers [57, 58, 66]. The ablation process at 1-kHz pulse repetition rate causes a considerable change to the surface properties of the target due to its melting, which deteriorates the plasma plume conditions during laser ablation. Surface heating and melting of a static target result in an unstable harmonic signal, so that movement of the target surface is required to maintain a reasonable stability. Demand to find the optimal way to improving plasma harmonic stability at a 1-kHz laser pulse repetition rate is high due to recent disclosure of the advanced properties of plasma harmonics over gas harmonics [62, 63, 67]. In particular, the plasma HHG conversion efficiency was measured one order of magnitude stronger than gas HHG efficiency [62]. Analogous features were reported in Ref. [67].

The obstacle to all plasma harmonic experiments in earlier studies was the insufficient stability of plasma parameters (density, ion and free electron concentrations, excitation conditions, etc), which led to an instability of harmonic yield and the fast decay of harmonic efficiency under irradiation of the same spot on the ablated target. As has already been mentioned, most of those early studies were performed using 10-Hz class lasers. At this relatively low pulse repetition rate, the stability of the harmonic generation deteriorated after a few hundred shots on the same spot of the surface and even more quickly for powder-like materials (fullerenes, nanotubes, metal nanoparticles, various organic and inorganic powders). One can note that laser ablation of the latter samples can be considered an important tool for their structural studies using XUV nonlinear spectroscopy. The application of soft ablation allows the employment of the same target for a much longer period than in earlier studies of overexcited targets during laser ablation. Thus, the search for a robust, easy-to-apply method allowing one to improve the harmonic stability in plasma HHG could considerably advance the search for the fundamental (structural, orientational, etc.) properties of organic and inorganic atoms and molecules.

The approaches used earlier and based on a rotating disc geometry [25, 68, 74, 144] permitting the movement of targets during ablation are not suitable, since the distance between the driving femtosecond laser beam and target surface should be maintained at a minimum (around 100 μm), while the Rayleigh length of the driving beam is maintained within the range of a few millimeters. Below, we describe a new method designed around a motorized rotating rod specifically prepared for HHG from plasma plumes using high pulse repetition rate lasers, and we demonstrate that this target significantly improves the stability of high-order harmonics [72].

Those studies were performed making use of two laser pulses: one to produce the plasma plume on the rotating rod, and the other to drive the HHG at its action. The first (heating) pulse was created by splitting off a portion ($E = 200$ μJ) of the uncompressed 8-ps laser pulse from a

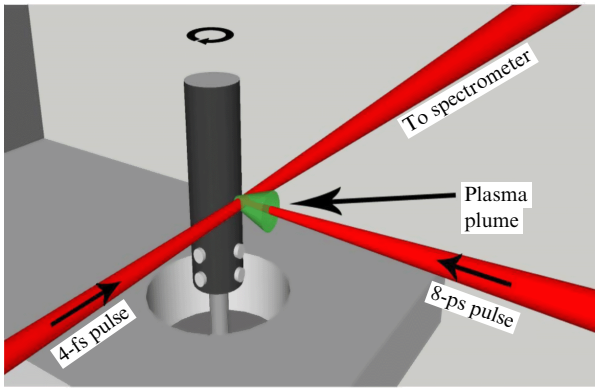

Figure 14. Schematic of a rotating target and HHG configuration [72].

1-kHz Ti:sapphire chirped pulse amplification laser. The remaining pulse was compressed in a prism compressor and then further compressed with the aid of a hollow fiber and chirped mirrors, resulting in 250-μJ, 3.5-fs pulses. The driving (probe) pulse was delayed with respect to the heating pulse by 40 ns to give the plasma time to expand away from the target surface, thus allowing the probe pulse to pass through the plasma without being clipped by the target.

A target rotation apparatus consisted of three linear stages driven by stepper motors along three axes. The target was attached to an axis of a fourth motor which provided rotation with a variable speed (from a few rotations per minute (rpm) up to 300 rpm). Such a mode of the target rotation was sufficient to achieve stable harmonic emission, and an additional vertical movement was not required, though this capability might be useful for future plasma HHG experiments. As the setup requires the target to be positioned very close to the driving beam, it was of paramount importance that the target be carefully aligned with the axis of rotation. Any movement of the target surface due to eccentricity in the radial direction from the driving beam axis would result in an oscillation of the harmonic signal caused by variations of the plasma density seen by the driving beam or, in the extreme case, by partial clipping of the laser beam.

The target (cylindrical rod with a diameter of 10 mm and length of 30 mm) was positioned as shown in Fig. 14, with the probe pulse axis propagating 100–200 μm above the target surface. The picosecond heating pulse was focused onto the surface of the rotating target. In order to efficiently produce high-order harmonics, the plasma had to be weakly ionized [139]. To achieve this, the target was positioned slightly in front of the focus of the heating pulse using a 50-cm focusing lens, leading to an on-target laser radiation intensity of $\sim 1 \times 10^{10}$ W cm^{-2}. This also had the benefit of increasing the size of the plasma plume produced from ablating a larger target area. The size of the focus on the target surface was measured to be ≈ 500 μm. The delayed probe pulse was focused through the plasma with the aid of a 40-cm spherical mirror. The HHG radiation was analyzed by an XUV spectrometer consisting of a flat-field grating and an imaging microchannel plate detector with a phosphor screen imaged onto a CCD camera.

Figure 15 shows that there is a drastic change in the harmonic signal (integrated over the spectral range of 40–80 nm) when the rotation of the aluminum target is stopped. A sharp harmonic intensity decrease of more than one order

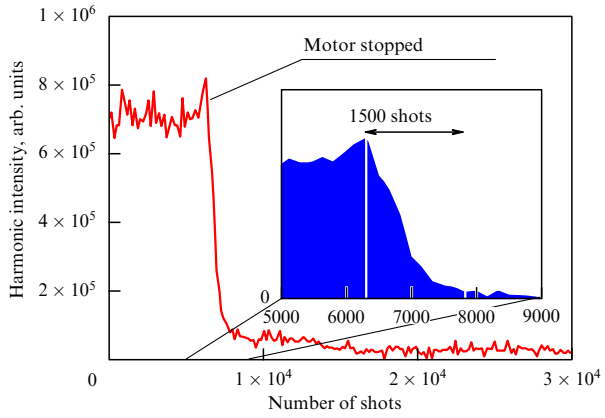

Figure 15. Decay of the harmonics from aluminum plasma after stopping the rotation of the motor. The generated harmonics were integrated over the 40–80 nm spectral range [72].

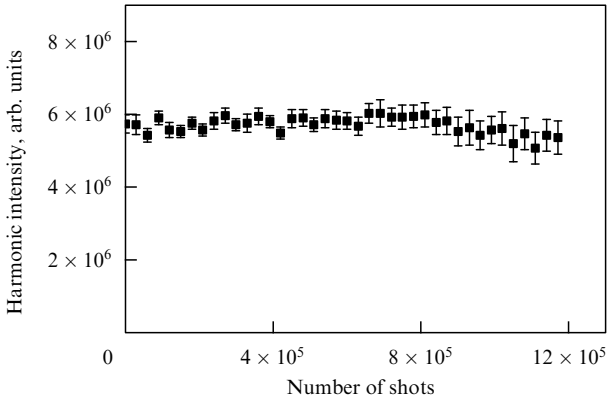

Figure 16. Stability of an integrated harmonic signal generated in an aluminum plasma in the case of a rotating target [72].

of magnitude over only one thousand shots (or just after one second of ablation using a 1-kHz laser) is observed. The benefits of the rotating rod are clearly shown in Fig. 16, where stable harmonic generation was achieved from the plasma created on an aluminum target for over 1 million laser shots. Stable harmonics were produced in a broad range of the rates of rotation (10 rpm and faster). The target rate of rotation and the size of the ablation focus imply that the same area of the target was undoubtedly used repeatedly for consecutive rotations over the 20 minute duration of the experiments. This could have resulted in thermal damage issues with this high pulse repetition rate.

It is probable that once the fixed surface starts to melt, the action of a following laser shot and plasma creation could expel some of the liquid target layer from the ablation area, which would not cause the plasma to be ejected in a direction normal to the surface. These effects are considerably diminished once the target starts to rotate. During rotation, the previously ablated area cools down such that, during the next set of ablation on this spot, plasma formation occurs in approximately the same conditions. To prove that the ablated area cools down with rotation, the target was rotated at different rates (from 10 to 300 rpm), and no difference in the stability of the harmonic yield was found. These observations point out the importance of periodic changes to the ablation zone. This also confirms a suggestion that the cooling of the ablation area leads to stable plasma creation.

The plasma characteristics (such as density and degree of ionization) are the most important parameters for achieving and maintaining stable HHG efficiency during an extended period of laser illumination. Calculations [67] have shown that, in carbon-ablated plasma, the concentration of particles in the area of femtosecond laser–plasma interaction with an optimal delay between heating and probe pulses (~ 40 ns) is amounted to $\sim 2 \times 10^{18}$ cm^{-3}. The solid surface was considered as the one unheated before laser ablation. Indeed, after one round of rotation (e.g., after 0.2–2 s), the plasma disappears, the ablated spot cools down, and the next laser shot on the same spot can be considered as a shot on a nearly 'fresh' surface. In contrast, the following shots in the case of a stationary target continue the heating of the same spot.

The novelty of this approach also includes the imparting of advanced properties to plasma HHG even at extremely small energies of the heating pulses. The efficiency of plasma HHG depends on the possibility of creating 'optimal' plasma. This can be done using both multi-mJ laser pulses, as was shown in previous studies [4], and a few hundred μJ pulses, as was demonstrated in the reviewed work [72] and recently published studies [67]. The important point here is the intensity and fluence of the heating pulse on the target surface. The application of a higher-energy heating pulse could create the conditions for an 'optimal' plasma over a longer distance, which could (or could not) increase the harmonic yield, depending on the phase relations between the probe and harmonic waves. In addition, it can also lead to the overheating of the target at 1-kHz ablation. As mentioned above, the rate of rotation did not influence the stability of the harmonic generation with 0.2-mJ heating pulses. The use of more energetic pulses (i.e., on the order of a few mJ) at a high repetition rate may require additional optimization of the rotation target technique (for example, by periodic up and down dragging of the rotating target).

7. High-order harmonic generation in graphite plasma plumes using ultrashort laser pulses: a systematic analysis of harmonic radiation and plasma formation conditions

As noted above, the characteristics of laser plasma play a crucial role in determining how efficiently higher harmonics can be generated in the plasma plumes. An increase in the free electron density is likely to have been the limiting factor for the harmonic cut-off energy in early experiments with laser plasmas [22, 24, 25]. A search for appropriate target materials, which can provide favorable ablation plasmas for efficient HHG, has motivated the analysis of plasma characteristics under conditions of a high yield of harmonics. Recent studies have shown that carbon-ablated plasmas are a promising media to satisfy the above requirements [63, 67].

Shot-to-shot stability of the harmonic signal is also crucial for any application of the generated radiation and especially for the measurement of the pulse duration of converted XUV radiation. Such temporal HHG measurements were taken on chromium plasma [62]. Using the reconstruction of attosecond beating by interference of two-photon transitions (RABITT) technique, the authors showed that the set of 11th–19th harmonics of a Ti:sapphire laser form, in the time domain, an attosecond pulse train (see also Section 3). It was underlined that instability of the harmonic signal in their experiments utilizing a 10-Hz pulse

repetition rate laser was the main obstacle to an accurate measurement of the temporal structure of plasma-generated harmonics. Besides its fundamental interest, high-order harmonic generation in plasma plumes could thus provide an intense source of femtosecond and attosecond pulses for various applications.

Optical parametric amplifiers (OPAs) operating in the mid-infrared (MIR) range are promising tools for harmonic cut-off extension and attoscience experiments. The spectral cutoff energy of HHG obeys the scaling law $E_c \sim I\lambda^2$ [28], where I is the peak intensity of the probe laser field, and λ is its central wavelength, which allows one to extend the harmonic emission beyond the 100-eV range by using longer-wavelength laser sources. Another advantage of mid-infrared optical parametric amplifiers (MIR OPAs) is their wavelength tuneability, which allows one to tune the spectral position of harmonics towards ion radiative transitions with strong oscillator strengths. This feature allows the observation of resonance-enhanced harmonics and broadens the range of plasma samples where this phenomenon could be realized, compared with $\sim$ 800-nm lasers with an essentially fixed wavelength [136]. Moreover, by taking advantage of two-color HHG techniques, the application of MIR OPAs allows the investigation of complex molecules during their ablation and HHG using tuneable long-wavelength radiation. These features are interesting for spectroscopic applications of HHG in the MIR range [145, 146].

In the meantime, the employment of MIR OPAs for HHG should lead to a reduced harmonic generation efficiency that scales as λ^{-5} [147, 148]. It is of a considerable interest to analyze the relative behavior of plasma harmonics for 800-nm and MIR lasers, and thereby to find the conditions when the reduction in harmonic yield becomes not so dramatic due to some enhancement mechanisms, such as the presence of *in situ* produced nanoparticles, which increase the HHG conversion efficiency. It is worth noting that previous studies of plasma HHG in carbon plumes [63] have inferred, through analyses of plasma debris morphology, the formation of nanoparticles during laser ablation of carbon-containing targets.

Atomic carbon is a reactive species which ensures stability of various multiatomic structures with different molecular configurations (allotropes). All the allotropic forms of carbon (graphite, diamond, and amorphous carbon) are solids under normal conditions, but graphite exhibits the highest thermodynamic stability. Laser ablation of graphite has been intensively examined during the last ten years to define plasma conditions for the synthesis of carbon structures with unique properties. The physical characteristics of the plasma plume, such as concentrations of atoms and clusters, directly affect the properties of the material being formed in the dynamic expansion of the ablated material. The successful synthesis of clusters is strongly dependent on the formation of atomic and molecular species with the required chemistry and aggregation ability. Thus, to select the optimal plasma conditions for HHG, a detailed understanding of the basic physical processes governing the ablation plume composition and reliable methods for controling the plume species are needed. The reasons mentioned above and the consideration of recent studies of HHG in carbon plasmas [63], as well as recently reported comparisons of the HHG in graphite-ablated plasmas and argon gas [64, 67], have prompted the systematic analysis of the plasma creation conditions for achieving optimal HHG conversion efficiency in graphite plasmas [73].

7.1 HHG in carbon plasma under various conditions

High-intensity few-cycle pulses (760-nm central wavelength, 0.2 mJ, 3.5-fs pulse with 1-kHz repetition rate) were typically obtained from the Ti:sapphire laser after the second stage of compression consisting of hollow fiber filled with neon and a bunch of chirped mirrors [149]. The compressed pulses were characterized by a spatially encoded arrangement for direct electric field reconstruction by spectral shearing interferometry. This radiation was harnessed for frequency up-conversion in the specially prepared carbon plasma. A portion of the uncompressed radiation of this laser (central wavelength 780 nm, pulse energy 120 μJ, pulse duration 8 ps, and pulse repetition rate 1 kHz) was split from the beam prior to the laser compressor stage and was focused into a vacuum chamber to heat the graphite target and create plasma on its surface (Fig. 17). These picosecond heating pulses were focused by a 400-mm focal length lens and created a plasma plume with a diameter of $\sim$ 0.5 mm at a laser radiation intensity $I = 2 \times 10^{10}$ W cm^{-2} on the target surface. The time delay between plasma initiation and femtosecond pulse propagation origin was fixed at 33 ns. As an alternative ablation, 10 ns, 1064 nm pulses from a 10-Hz repetition rate Q-switched Nd:YAG laser were utilized, which provided an intensity 1×10^9 W cm^{-2} on the target surface. The time delay between the 10-ns heating pulses and the 3.5-fs probe pulses was varied here in the range of 10–60 ns to maximize the harmonic yield.

The 3.5-fs probe pulses propagating in a direction orthogonal to that of the heating pulses were focused into the laser plasma with the aid of a 400-mm focal length reflective mirror. The position of the focus with respect to the plasma area was chosen to maximize the harmonic signal, and the intensity of femtosecond pulses in the plasma area under these conditions was estimated to be $I = 6 \times 10^{14}$ W cm^{-2}. The 30-fs, 780-nm, 2-mJ probe pulses from another Ti:sapphire laser operating at a 1-kHz repetition rate and producing approximately the same radiation intensity inside the laser plasma were also used for HHG. The details of this setup and registration system are presented in Refs [67, 69].

In order to analyze the harmonic yield of the MIR source in the graphite-ablated plasma, an OPA pumped by a 30-fs Ti:sapphire laser was employed. A beam splitter inserted in front of the laser compressor of this Ti:sapphire laser allowed picking off 10% of the laser beam (780 nm, 1 mJ, 160 ps, 1 kHz pulses) to generate a plasma plume on the graphite targets,

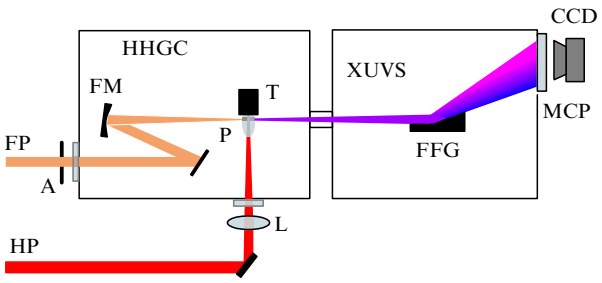

Figure 17. Experimental setup for harmonic generation studies in plasma plumes: FP, femtosecond probe pulse; HP, picosecond heating pulse; A, aperture; HHGC, high-order harmonic generation chamber; FM, focusing mirror; L, focusing lens; T, target; P, plasma; XUVS, extreme ultraviolet spectrometer; FFG, flat field grating; MCP, microchannel plate and phosphor screen detector, and CCD, CCD camera [73].

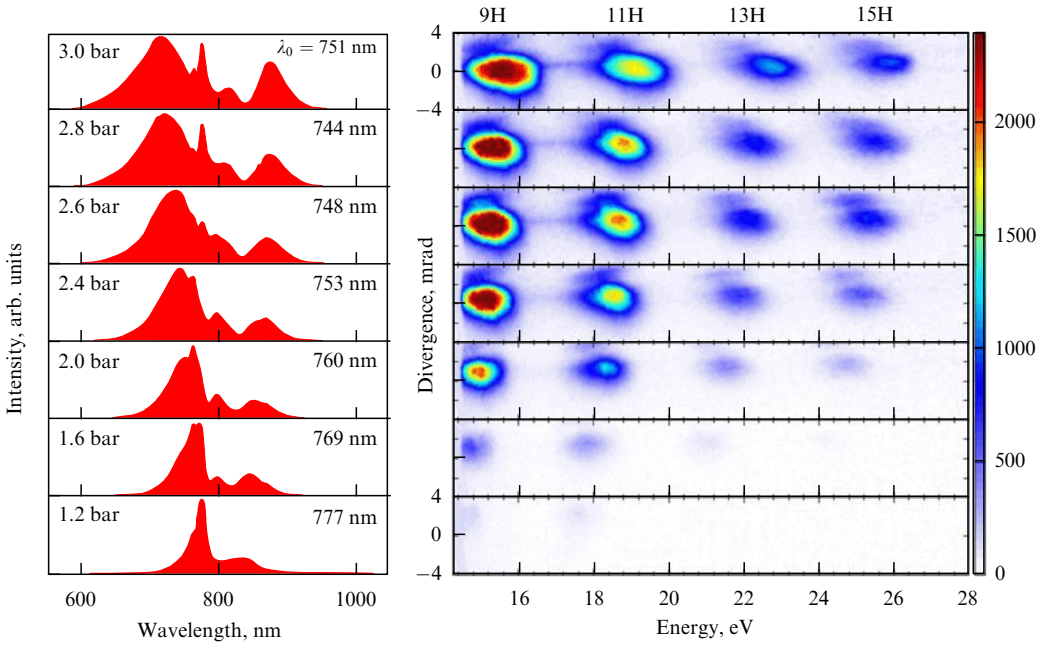

Figure 18. (Color online.) Carbon harmonic spectra as a function of neon pressure in a hollow fiber. The corresponding harmonic spectra measured in front of the vacuum chamber are presented on the left panel. The plasma was created using 10-ns pulses. λ_0 stands for a weighted average wavelength of the spectral distribution. The color scale indicates the harmonic intensity [73].

with the remaining 90% being compressed to 30 fs (7 mJ) for pumping a commercial OPA. The OPA was optimized for high conversion efficiency, beam quality, and duration of the converted pulses. To achieve high reproducibility of the generated pulses, all the amplification stages were driven to saturation. This device generated 35-fs pulses tunable in the 1200–1600 nm range. The idler pulse covered the 1600–2200 nm range. The time delay between the heating ablation pulses and MIR pulses from the OPA was set to 35 ns, as this delay was found to be optimal for the efficient generation of highest harmonics.

Since the goal of these studies consisted in analyzing the graphite-ablated plasma characteristics under the conditions of efficient HHG of ultrashort laser pulses, this process was first optimized by achieving the maximum conversion efficiency and highest harmonic cut-off using the probe radiation from both the Ti:sapphire lasers with fixed wavelengths and the tunable OPAs. Efforts were then concentrated on the analysis of the 'optimal' plasma plume applying three measuring techniques: optical emission spectroscopy of emitting plasma species in the visible, UV, and XUV spectral ranges; scanning electron microscopy for inspection of deposited plasma debris, and, finally, time-of-flight mass spectrometry for analyzing the ionic components of the plasma.

To analyze the influence of the spectro-temporal characteristics of the probe laser radiation on the harmonic yield, the backing pressure of neon in the hollow fiber of a second compressor was changed, which allowed varying pulse duration from 25 to 3.5 fs [150]. The dependences of the spectral and intensity characteristics of the harmonic images recorded by the CCD camera in the 15–25 eV range on different input pulse spectra and backing pressures of neon are displayed in Fig. 18. One can clearly see that, with an increase in backing pressure (from 1.2 to 3 bar), the harmonic intensity increases, while the harmonic wavelength spectrally shifts towards the blue side. During these experiments, the driving pulse energy was held constant.

An interesting feature of the carbon harmonic spectrum from 10-ns pulse-induced plasma is that the spectral width is about 2–3 times broader than that of harmonics generated in other atom- and ion-rich plasmas at the same fluence and intensity of heating pulse, when using few-cycle pulses. For example, the full width at half maximum for medium-order harmonics reached 1.5 nm for graphite plasma versus 0.4 nm for different metal (Ag, Al, and Cu) plasmas. The broader width of the harmonics can be explained by self-phase modulation and chirping of the fundamental radiation propagating through the carbon plasma. The presence of nanoparticles in the plasma plume may also contribute to bandwidth broadening of harmonics.

For practical applications of the coherent short-wave radiation generated in graphite plasma utilizing a 1-kHz pulse repetition rate driving laser, it is necessary to analyze the stability of the plasma characteristics and the generated harmonics. A recently introduced new technique for maintaining a stable ablation plasma in harmonic generation with high pulse repetition rate lasers (> 1 kHz), which is built around a cylindrical rotating metal target [72], was described in the previous section. The studies under discussion [73] have shown that, in spite of the different properties of metal and graphite targets, the rotating target allowed achieving stable HHG in both metal and graphite plasmas. The rotating graphite rod makes it possible to maintain a relatively stable harmonic yield well above 1×10^6 laser shots. Harmonics up to the 29th order were routinely observed in those studies using 3.5-fs laser pulses.

Figure 19a displays the harmonic spectrum generated in the case of 1300-nm probe pulses. Harmonics up to the 59th order were observed in conditions of carbon plasma formation by heating with uncompressed 160-ps pulses from this laser. It is worth noting that the application of less intense 1400-nm pulses available by tuning the OPA, while generating weaker harmonics, did not result in a higher harmonic cut-off than in the case of 1300-nm pulses. This inference suggests that the harmonic generation occurred under

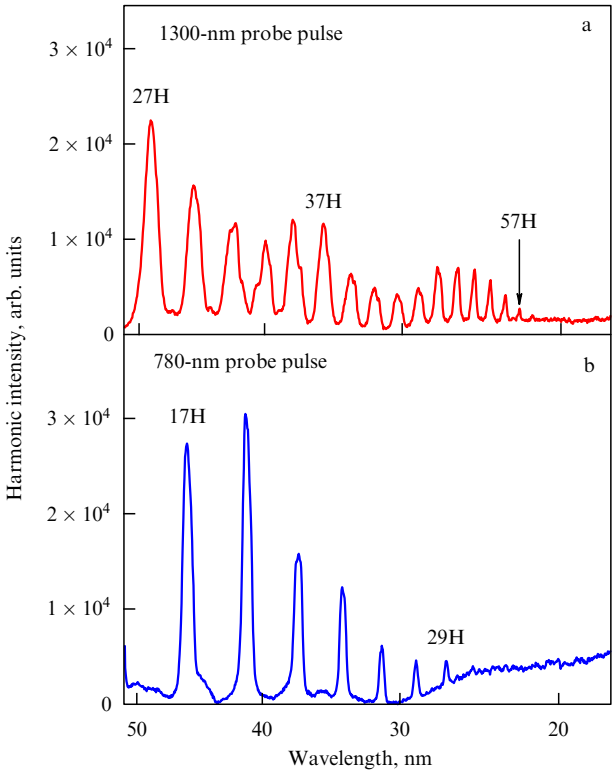

Figure 19. Plasma harmonic spectra taken using 1300-nm (a) and 780-nm (b) probe pulses. The energies of the probe pulses were 0.2 mJ (a) and 0.54 mJ (b). Ablation was performed with the aid of 160 ps, 780 nm, 1 kHz laser pulses [73].

saturated conditions, with the expectation of even stronger harmonics once the micro- and macroprocesses governing frequency conversion are optimized.

Harmonic spectra of up to the 29th order in the case of 780-nm, 30-fs probe pulses are presented in Fig. 19b. By comparing these data with the spectra collected for a 1300-nm driving source (Fig. 19a), one can clearly see the expected extension of harmonic cut-off in the case of the longer-wavelength radiation being converted. The important peculiarities of these comparative studies are the broadband harmonic spectra obtained with the 1300-nm laser and a similar yield of harmonics at the two driving wavelengths. Whilst the former feature depends on the bandwidth of the OPA output, the latter observation requires additional consideration. The plasma harmonic yield from the MIR source did not follow the expected $I \propto \lambda^{-5}$ rule. In fact, for the intensities of the MIR and 780-nm pulses involved [$\sim (2-4) \times 10^{14}$ W cm^{-2}], the harmonic generation efficiency of the XUV radiation driven by MIR pulses was higher than in the case of 780-nm pulses, while supplying the lower energy of the former pulses (0.2 and 0.54 mJ, respectively). It should be noted that the $I \propto \lambda^{-5}$ rule predicts a $\sim$ 13-fold decrease in conversion efficiency for the MIR (1300 nm) pulses compared to that with 780-nm pulses at equal probe pulse intensities.

7.2 Characterization of optimal plasma formation conditions

This section is concerned with the characterization of graphite-ablated plasma plumes in conditions of maximum HHG conversion efficiency. In graphite, the ablation plasma plume may contain various species of carbon, e.g., neutrals and ions, small molecules, clusters, aggregates, etc., which can contribute to harmonic generation to various extents. It is important to determine their presence in the region where the driving laser pulse interacts with the expanding plasma. In particular, the production of clusters in the laser plasma during laser ablation of various targets has a high probability, while their presence and concentration in the plasma area where the frequency conversion occurs is yet to be confirmed directly. Another issue resolves itself into the question of how one can define the density of monomers, dimers, and clusters and their influence on the HHG yield. Analysis of post-ablation conditions of the deposited debris can provide information on the nature of those species, despite the differences between the composition of the plasma formed at its early stages and the deposited material, due to the influence of aggregation on the substrate [151]. One more issue of interest is whether the spectral characterization of the plasma emission in the visible and UV ranges can provide some clues about the plasma conditions, without a simultaneous analysis of the XUV emission.

Plasma characterization through optical spectroscopic measurements in the visible, UV, and XUV ranges in conditions of different HHG efficiencies was carried out with the aid of the above XUV spectrometer (see Fig. 17) and a fiber spectrometer. The fluences of heating pulses at which the spectra were recorded corresponded to both optimal and nonoptimal conditions of HHG. The acquisition times were set to 1 s for measurements of XUV spectra, and to 0.5 s for measurements of visible and UV spectra. The characterization of plasma debris collected on silicon wafers placed 4 cm away from the ablated target was performed by scanning electron microscopy.

Cluster composition of the ablation plume produced by nanosecond laser pulses was investigated by time-of-flight mass spectrometry (TOFMS). A brief description of the experimental setup is given here; more details of the TOFMS can be found elsewhere [152]. The laser beam (1064 nm, 5 mJ, 10 ns pulse duration) was focused at normal incidence onto a 2-mm spot at the surface of the graphite target. The laser intensity on the target surface was 1.5×10^9 W cm^{-2}, which resulted in the creation of an optimal plasma for efficient HHG using nanosecond ablation pulses. The target was placed in a vacuum chamber (pumped down to $\sim 2 \times 10^{-6}$ bar) between the extracting and accelerating plates of a linear TOFMS. The target surface was parallel to the flight axis of the spectrometer. The target could be rotated and displaced at variable distances from the axis. Positive ions produced in the ablation were deflected along the TOFMS axis by an electric field typically in the range of 300–400 V cm^{-1} and accelerated by a total voltage of 2500 V. A high-voltage switch was used to apply the bias voltage at controlled delays with respect to the laser ablation pulse. Ions entered the drift region (flight length of $\sim$ 1 m) and were detected by a microchannel plate. Analysis of neutral species produced in the ablation could also be performed by making use of a second postionization laser source (excimer F_2 laser irradiating at $\lambda = 157$ nm). The postionization laser pulses interacted with the ablation plume perpendicularly to the plume propagation axis, at different distances from the target surface and at different time delays with respect to the ablation laser irradiation.

It has been shown previously that efficient harmonic emission is only observed when the visible and UV plasma emissions are dominated by neutral and singly ionized carbon

lines [139]. The present studies [73] have also confirmed this feature at the optimal laser fluence providing the target surface heating. The broad features of emission spectra near 470, 515, and 555 nm could be assigned to the bands of excited C_2 molecules. These bands have also been recorded in early studies of the graphite ablation (see, for instance, Refs [153–155]). Other lines in the spectra were attributed to carbon neutrals and singly charged ions.

The analysis of optical spectra in the visible and UV ranges does not provide information about the presence of highly ionized species which can be revealed by collecting the plasma emission in the XUV range. The XUV spectrum of carbon plasmas, taken following excitation by an 8-ps heating pulse at high intensity, but without further excitation by the probe pulse, provides some insight into the plasma components prior to interaction with the driving radiation. This spectrum was recorded under conditions of a considerable decrease in the nonlinear optical response of the medium (i.e., at weak HHG) and revealed the appearance of many emission lines from C II and C III ions. Overexcitation of the target by 10-ns pulses also led to the appearance of emissions from highly charged (C III, C IV) ions.

It should be noted that those measurements were time-integrated, so one could not say exactly which plasma components existed at the moment of the propagation of the femtosecond beam through the plume. However, the presence of ionic lines from multicharged species in the last two cases gives a strong indication of overexcitation of the target and of its negative influence on HHG efficiency. One can note that, at this level of excitation of the graphite-ablated plasma, harmonic generation was partially or entirely suppressed. Specifically, a two-fold increase in the intensity of 8-ps pulses (from 2×10^{10} to 4×10^{10} W cm^{-2}) led to a decrease in harmonic intensity by a factor of 2.5. The same can be said about the excitation by longer (10 ns) pulses, though the threshold, at which harmonics started to decay, was considerably lower (2×10^9 W cm^{-2}). Application of 10-ns pulses with an intensity of 3×10^9 W cm^{-2} led to a substantial decrease in harmonic generation efficiency and to the appearance of emission lines from highly charged ions. One can notice that, under conditions of efficient HHG, no ion emission lines appear alongside the harmonic spectra.

To prove the presence of clusters in carbon-ablated plasmas under optimal conditions of harmonic generation, the morphology of deposited debris from graphite plasma created during target surface ablation by picosecond and nanosecond pulses was analyzed. It has already been mentioned that laser ablation of a solid material is a widely accepted technique for the generation of nanoparticles. However, this process has previously been studied without taking into account the role of free electrons and highly excited ions, which violate the optimal conditions for phase-matched HHG. SEM measurements of the deposited debris were carried out under laser ablation conditions corresponding to the optimal plasma formation for efficient HHG. The substrates (glass plates and silicon wafers) used to collect the deposited material were placed at a distance of 40 mm in front of the ablation area, and the debris was further analyzed by SEM.

Under optimal carbon plasma formation conditions, when the highest harmonic conversion efficiency was achieved with 8-ps ablation pulses, the SEM images did not reveal the presence of nanoparticles in deposited debris with sizes above the microscope detection limit (5 nm). This was

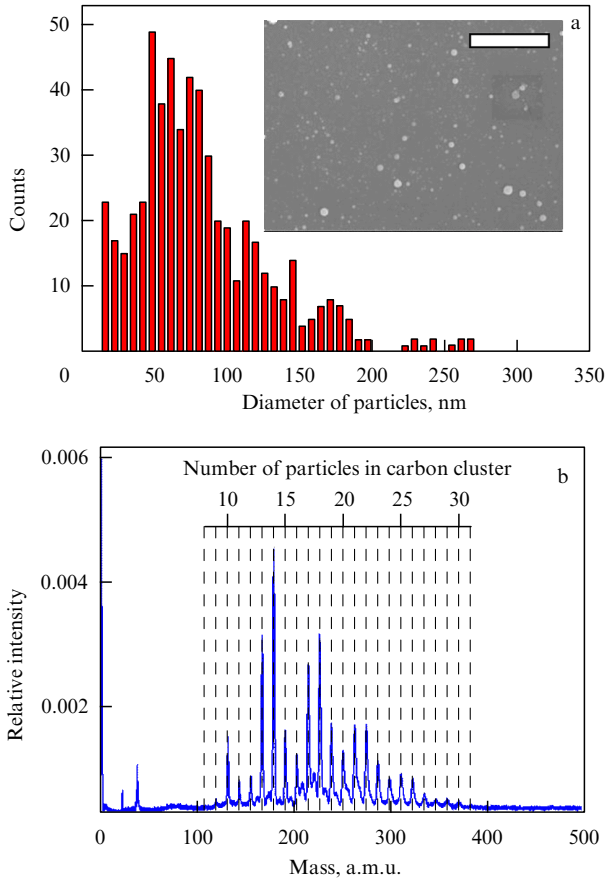

Figure 20. (a) Histogram of the size distribution of deposited nanoparticles and corresponding SEM image of deposited debris in the laser ablation of a graphite target with 10-ns pulses. The size bar in the SEM image is 2 μm. (b) Mass spectrum (in atomic mass units) of carbon plasma obtained during excitation of a graphite target using 10-ns pulses in conditions close to optimal plasma formation for HHG [73].

probably due to the small fluence (0.2 J cm^{-2}) of the heating radiation on the target surface ($I = 2.5 \times 10^{10}$ W cm^{-2}). It is possible that in carbon plasmas produced at these conditions, the harmonics could also originate from nanoparticles with sizes below the detection limit. Another pattern was observed upon ablation of the target with 10-ns pulses, where considerably higher heating fluence (10 J cm^{-2}) caused the appearance of nanoparticles deposited onto a nearby substrate. In relatively moderate conditions of laser ablation with 10-ns pulses ($I \approx (1-2) \times 10^9$ W cm^{-2}), a high density of nanoparticles appeared in the SEM images of the deposits, with their sizes mostly distributed in the range between 10 and 200 nm around the mean size of about 50 nm (Fig. 20a). One has to reiterate that these debris characteristics were measured at the maximum conversion efficiency for the 15th–23rd harmonics. These morphological studies confirmed the presence of relatively large nanoparticles deposited onto the substrates under conditions of 'optimal' laser ablation with 10-ns pulses. However, some uncertainty still remains about the correlation of these results with the presence of the same nanoparticles in carbon plasma during harmonic generation, due to the possibility of their aggregation into clusters after deposition. To address this issue, the TOFMS of nanosecond pulse-ablated graphite was carried out.

Figure 20b displays the mass-resolved spectrum of carbon plasma after 60 shots of 10-ns heating pulses. Those studies

Table 3. Calculations of carbon plasma concentrations for different intensities of 8-ps and 10-ns laser pulses heating a graphite target.

Intensity, 10^9 W cm^{-2}	Plasma concentration, 10^{17} cm^{-3}	
	8 ps	10 ns
6.6	1.1	
20	2.6	
60	4.0	
0.33		10
1		25
3		37

revealed that, in plasma conditions close to optimal for HHG, the laser plume contains a group of small, singly ionized carbon clusters ($C_{10}-C_{30}$). Attempts to find higher-mass clusters failed, though a search for them was carried out over a longer range of time delays (up to a few μs) between the onset of laser ablation and the switching on of the triggering pulse in the TOFMS.

To ascertain the presence of neutral species in the ablated plasma using TOFMS, an additional source of ionization should be used. In the present case, an excimer F_2 postionization laser ($\lambda = 157$ nm) served that purpose. Photons with this wavelength can induce the ionization of neutral clusters through single-photon absorption. However, once the 157-nm pulse was focused on the plasma area, no evidence of neutral clusters in the mass spectra was found. This could be explained by the fact that the ionization potential of carbon atom ($I_i = 11.2$ eV) is higher than the photon energy of the ionizing laser ($E = 7.9$ eV) and by the difficulty of ionizing existing carbon clusters by two-photon absorption of 157-nm radiation, due to the low intensity of the latter in the plasma area.

The carbon plasma concentrations under the experimental conditions of target ablation (i.e., 2×10^{10} W cm^{-2} intensity in the case of 8-ps pulses, and 1×10^9 W cm^{-2} in the case of 10-ns pulses) allowing efficient harmonic generation were calculated using a three-dimensional molecular dynamics simulation of laser ablation of graphite based on the molecular dynamics code ITAP IMD [156]. The corresponding concentrations were found to be 2.6×10^{17} cm^{-3} and 2.5×10^{18} cm^{-3}. The results of calculations of carbon plasma concentration for different intensities of heating 8-ps and 10-ns laser pulses are summarized in Table 3.

7.3 Analysis of HHG and plasma characteristics

An earlier study suggested that the presence of nanoparticles in carbon laser ablation plasmas can explain the observed strong harmonic yield from these media [63]. It was reported that the debris from ablated graphite and carbon targets contained nanoparticles with sizes between 100 and 300 nm. The authors of Ref. [63] suspected, therefore, that nanoparticles formed in the plasma by ablation were the source of intense harmonics. Heterogeneous disintegration, liquid phase ejection and fragmentation, homogeneous nucleation and decomposition, and photomechanical ejection are among the processes that can lead to the aggregation and disintegration of nanoparticles [157–159]. A variety of different techniques were applied in those studies to determine the aggregation states of the evaporated material, including time-resolved emission spectroscopy, CCD-camera imaging of the plasma plumes, Rayleigh scattering, and laser-induced fluorescence.

In the earlier discussed work [73], SEM for debris analysis and TOFMS were applied for plasma characterization. These two methods have provided useful clues about the conditions and dynamics of a plasma plume formed above the target surface. Whilst the former method provided some information about the presence of nanoparticles in the plasma, one has to cautiously consider those results from the following point of view. The deposition process on the substrate happens much later than the time of HHG emission, and the physical process of deposition may lead to further aggregation. Since SEM is an *ex situ* method, one cannot rule out differences between the real composition of clusters in the plasma and the results of SEM measurements, although it clearly proves the presence of clusters in the plasma. TOFMS yields more information on the *in situ* presence of ionized clusters, although it requires ablation of the target under the same conditions as in HHG experiments and is not suited for the detection of neutral nanoparticles in the ablated plasma.

TOFMS measurements have not revealed the presence of neutral clusters in the plasma produced by 10-ns pulses for the reasons described in the previous section. However, other investigations (see, for example, Ref. [154]) based on two-photon ionization with an ArF laser (photon energy 6.4 eV) have indicated the presence of neutral carbon clusters. Early TOFMS studies of laser ablation of graphite have revealed the typical characteristics of the expanding plasma species (average velocity of 1.5×10^5 cm s^{-1}) and their concentration ($4 \times 10^{18} - 6 \times 10^{19}$ cm^{-3} [160]) in ablation with 532-nm, 10-ns pulses at fluences on the order of 3 J cm^{-2}. The measured mass distribution shown in Fig. 20b, revealing the presence of C_{10} to C_{30} species, is in good agreement with those observed in previous exploration of graphite-ablated plasma under similar excitation conditions [160]. The restriction of cluster sizes to small-sized carbon nanoparticles has also been reported in Ref. [161], where it was argued that stronger excitation conditions are needed for observing clusters larger than C_{32}. In that case, one should expect the appearance of closed cells made of joined five- and six-member rings. It was confirmed that C_{60} and C_{70} fullerenes are the most abundant species among the heavy ions of the carbon plasma plumes at high ablation fluences. It was also suggested in paper [160] that in all likelihood the plasma is sufficiently dense for cluster growth to occur via ion-molecular reactions. The kinetic mechanism can be responsible for the formation of carbon cluster ions, since the attendant supersonic entrainment model predicts considerable cooling down of the cluster ions. The cluster growth is based on the addition of many small carbon neutral species to the ions in a stepwise fashion.

An explanation for strong harmonic generation from nanoparticles compared with single atoms or ions could be the higher concentration of neutral atoms inevitably accompanying the presence of nanoparticles. The increase in electron–cluster pair recombination cross section as compared with atoms can also potentially enhance the HHG efficiency in nanoparticle-containing plasmas. Earlier studies of HHG from gases [146, 162, 163], as well as from plasmas containing various nanoparticles (Ag, Au, $BaTiO_3$, etc.) [136, 139], have proven these assumptions by demonstrating the enhanced HHG from clusters, as opposed to isolated atoms and ions. Further evidence for the cluster contribution to the enhancement of harmonic generation comes from investigations of very intense laser ablation of a silver target [51], which substantiated the assumptions regarding the participation of *in situ* generated nanoparticles.

The observation of a more extended harmonic plateau in the case of 1300-nm probe radiation also suggests the involvement of clusters in the HHG process with MIR pulses. Assuming the expected decrease in harmonic intensity from single-particle emitters with the growth of the driving radiation wavelength ($I \propto \lambda^{-5}$; see Refs [147, 148, 164, 165]), one can anticipate at least a one order of magnitude decrease in harmonic yield from MIR pulses compared to the harmonic yield obtained with 780-nm laser radiation under other equal conditions, in particular, pulse energy and duration. However, the experiment did not show a considerable difference between the intensities of harmonics originating from these two driving sources (see Fig. 19). The energy (0.2 mJ) of the 1300-nm pulses in the plasma area was even lower than that for the Ti:sapphire pulse (0.54 mJ). This inference suggests the involvement of a certain mechanism which compensates for the expected considerable decrease in harmonic efficiency for the longer-wavelength laser. The involvement of a cluster component of laser plasma in the process of frequency up-conversion may probably explain the observed inconsistency with the theoretical predictions of the $I \propto \lambda^{-5}$ rule derived for atomic species [166, 167].

In principle, the enhancement of the harmonic spectrum from the carbon plume in the 15–26 eV range may be explained by the involvement of surface plasmon resonances of nanoparticles, analogously to fullerenes [3] in the range of their giant resonance in the vicinity of 20 eV. To prove such a prediction in the case of carbon plasma, one should provide evidence of giant absorption in the above range, but this has not been reported yet in the literature. The plasmonic properties of carbon nanoparticles can be responsible for the observed enhancement of carbon harmonics; however, their role requires additional study. Another option for explaining the high harmonic generation yield from the carbon plume is the indirect involvement of the clusters in HHG, which, while not participating as harmonic emitters, could rather enhance the local field, analogously to recently reported studies utilizing gold nanostructures for enhancing gas HHG [166, 167].

As was mentioned, recent comparative studies of lower-order harmonic efficiency in argon gas and carbon plasmas have revealed stronger conversion efficiency in carbon plasmas [64, 67]. In this section, we have discussed evidence for the superior properties of graphite ablation for HHG. Some arguments which could explain the enhanced high-order harmonic yield from this medium are as follows: (a) the graphite target allows easier generation of a relatively dense carbon plasma and the production of adequate phase-matching conditions for lower-order harmonic generation; (b) the first ionization potential of atomic carbon is high enough to prevent the appearance of a high concentration of free electrons, a condition that is not necessarily met in metal plasma plumes; (c) neutral carbon atoms dominate in the carbon plume at optimal conditions of HHG before interaction with the femtosecond laser pulse, and (d) carbon species allow the formation of multiparticle clusters during laser ablation, which can enhance the HHG yield.

8. Isolated subfemtosecond XUV pulse generation in Mn-ablated plasmas

In this section, we discuss HHG from transition metal plasmas. These are very promising targets in view of the giant resonances found in their photoionization cross sections. For example, the Mn^+ cross section equals ~ 40 Mb at 50-eV photon energy [168], whereas rare gas atoms have cross sections between 1 and 8 Mb at this photon energy [169]. Photorecombination — the third step in the recollision model — makes up the inverse process of photoionization [170] and, therefore, HHG and photoionization must exhibit the same resonances. This has been confirmed not only by previous resonance-induced experiments with laser-produced transition metal plasmas but also in a recent study of HHG from xenon gas [171].

Resonance-induced enhancement of a single harmonic of the laser radiation allowed considerable improvement of harmonic generation efficiency in some specific XUV spectral ranges related to high oscillator strengths of a few ion radiative transitions in metals. This was confirmed in multiple studies following the initial observation of this phenomenon in indium plasma [30]. In particular, strong enhancement of a single harmonic was reported in Cr [33] and Mn [40] plasmas. The Mn plasma is of special interest, since it exhibited the highest harmonic cut-off energy observed in plasma plumes (101st harmonic of the Ti:sapphire laser [40]). In previous studies, multicycle (30 fs [40] and 140 fs [172]) laser pulses were employed and the generation of all harmonics in the plateau region was observed, together with strongly enhanced harmonics in the vicinity of 50 eV.

Recent progress in the generation of few-cycle pulses has allowed the observation of various new effects, including the realization of isolated attosecond pulse generation in gas media [173–175]. In this connection, it is interesting to analyze resonance-induced processes observed in an ablation plume using the shortest available probe laser pulses. Below, we present an analysis of the experiments on resonance enhancement in manganese-ablated plasmas with 3.5-fs probe pulses [129]. The most interesting feature observed in those experiments was a suppression of almost all neighboring harmonics in the vicinity of a resonantly enhanced single harmonic at the photon energy of ~ 50 eV (see also Section 4).

The experimental arrangements were analogous to those presented in Section 7 of this review (see Fig. 17). The harmonic spectrum in the case of propagating 3.5-fs pulses through the manganese plasma was strikingly different from other plasma samples (for example, Ag plasma) analyzed in separate experiments. While all other samples studied demonstrated a relatively featureless harmonic spectra with an extended cut-off (Fig. 21a shows the spectrum of the harmonics generating in silver plasma), the Mn plasma allowed the generation of a strong single harmonic substantially enhanced compared to neighboring ones (Fig. 21b).

As was already mentioned, the harmonic spectra from manganese plasmas for 30-fs and 140-fs laser pulses also showed enhanced harmonics around 50 eV. The assumption of the resonance nature of the enhancement of harmonics of the ~ 800-nm Ti:sapphire lasers in this spectral region is supported by the presence of a giant resonance in the vicinity of 50 eV, confirmed by experimental [168, 176] and theoretical [177] results. The enhancement of a single harmonic can be attributed to the broadband resonances in the ions of a few metals, such as V, In, Cd, Cr, and Mn. These 'giant' resonances have been experimentally confirmed in the literature [168, 176, 178] and discussed recently in a few theoretical studies [49, 111, 113, 114] (see also Section 4).

However, in previous studies [40, 172] involving multicycle probe pulses, the intensity of enhanced harmonics was

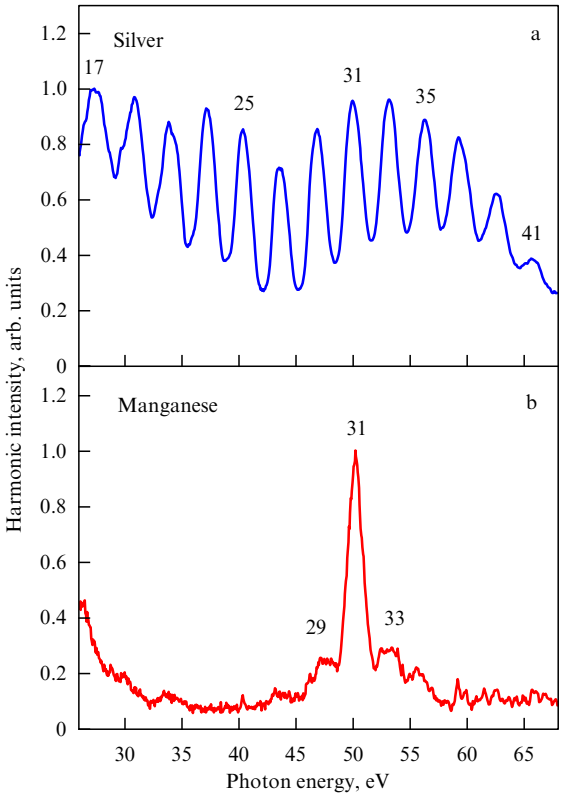

Figure 21. Harmonic spectra from (a) silver plasma, and (b) manganese plasma [129].

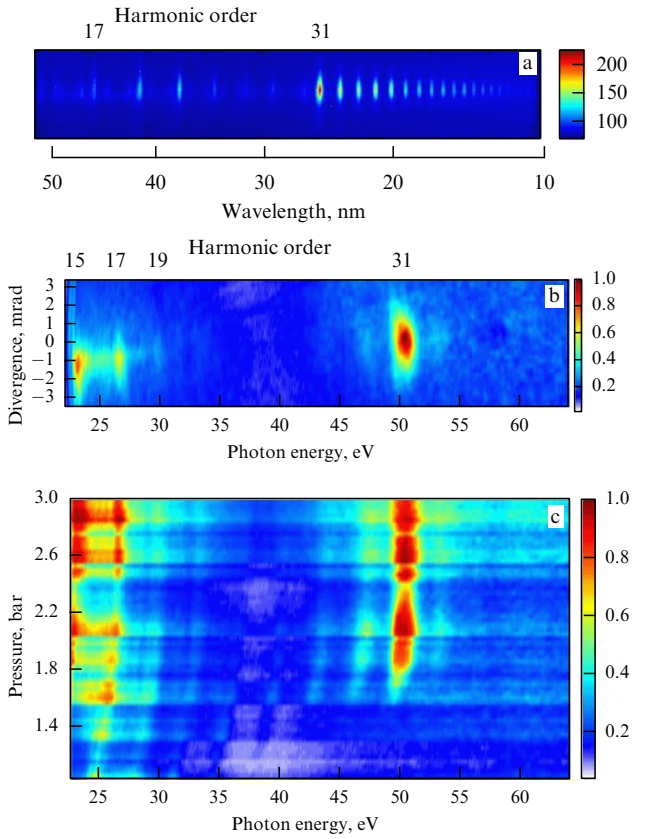

Figure 22. (Color online.) Raw images of harmonic spectra from manganese plasma in the case of (a) 40-fs, and (b) 3.5-fs probe pulses with the same intensity. (c) Raw images of harmonic spectra from Mn-ablated plasma at different pressures of neon in hollow fiber, taken at the same energy of probe laser pulses [129].

only a few times higher than those of neighboring-order harmonics. The same features were reproduced in the reviewed studies using 40-fs pulses from another Ti:sapphire laser at a similar radiation intensity (4×10^{14} W cm^{-2}) inside the laser plasma. The raw image of the harmonic spectrum presented in Fig. 22a shows several enhanced harmonics from the 31st order up to an extended second plateau. The extension of the harmonic cut-off exceeding the 71st order is attributed to the involvement of doubly charged Mn^{2+} ions as the sources of HHG. This feature of Mn plasma harmonics has already been reported earlier [40]. Also presented here is a typical pattern of an Mn harmonic spectrum for 3.5-fs probe pulses (Fig. 22b). No second plateau, which was seen in the case of multicycle (40 fs) pulses, is observed for a few-cycle pulse. Most striking was the observation of a single, very strong broadband (2.5 eV) 31st harmonic. Only two weak neighboring harmonics (around the strong emission line) are seen in the 30–65-eV spectral range. The ratio of the intensities of the enhanced harmonic to the weak neighboring harmonics exceeded one order of magnitude. One can note that, at a low intensity ($< 2 \times 10^{14}$ W cm^{-2}) of the femtosecond pulse, this strong harmonic disappeared when using both multi- and few-cycle pulses.

The distinctive structure of the harmonic spectra, taken both for 40-fs and 3.5-fs probe pulses, clearly points to the involvement of Mn ion resonances centered around 50–51 eV. The same can be said about the photoionization or photoabsorption characteristics of Mn^+ plasma, which are due to the 'giant' 3p $\rightarrow$ 3d resonance [168]. The laser pulse polarization dependence of this emission was analyzed, and it was found that the 50-eV radiation abruptly disappears with a change in the polarization state of the femtosecond probe pulses from linear to elliptical, which is a clear signature of the emission being due to high-order harmonic generation.

To analyze the effect of the spectro-temporal characteristics of the femtosecond radiation on the harmonic yield, the pressure of neon in the hollow fiber of a second compressor was varied, thus changing the duration of the harmonic-driving pulse [140]. The spectral and intensity variations of manganese harmonic spectra in the range of 22–62 eV as functions of neon pressure in the hollow fiber are depicted in Fig. 22c. One can clearly see that, with a change in pressure (from 1 to 2.3 bar), the single 31st harmonic intensity varies from almost zero to its maximum high value. A blue side shift of the generated harmonics is also evident. A further increase in the neon pressure up to 3 bar, at which the experiments with the 3.5-fs pulses were carried out, did not change the harmonic distribution.

The experiments described above were conducted without carrier envelope phase stabilization (namely, for random CEP values). The HHG experiments with Mn plasma using 3.5-fs pulses were also performed with stabilized CEP (e.g., at phases values of $\varphi = 0$ and $\pi/2$), and no considerable differences were found in that case (Fig. 23), though some variation of harmonic distribution was observed for the lower-order harmonics (cf. the middle and bottom curves in Fig. 23b, c). The spectral shapes of the 31st harmonic emission were quite similar at these two fixed values of CEP, while a considerable difference in harmonic spectra was maintained when compared to a longer pulse duration and lower intensity of the driving pulses. Figure 23 illustrates

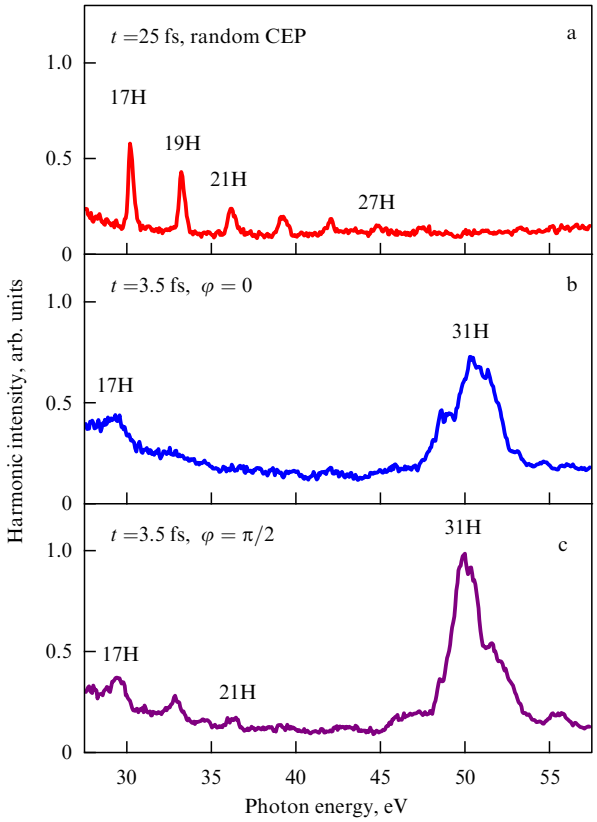

Figure 23. Experimental spectra of harmonics generated from manganese plasma in the absence of gas in a hollow fiber compressor ($t = 25$ fs) and random CEP (a), and at 3-bar pressure ($t = 3.5$ fs) at fixed CEP [$\varphi = 0$ (b); $\varphi = \pi/2$ (c)]. φ denotes the carrier envelope phase [129].

results of HHG measurements for 25-fs pulses (a) and 3.5-fs pulses (b, c) with the same energy (0.2 mJ). One can clearly see the absence of harmonic plateau extension and resonance-induced HHG in the case of low-intensity 25-fs pulses.

The fact that a strong CEP dependence of the plasma harmonic spectra in the case of 3.5-fs pulses was not observed could also be attributed to the presence of a significant number of free electrons in the manganese-ablated plasma, which might diminish the difference between the HHG spectra recorded for different values of CEP. The same can be said about other HHG experiments utilizing silver and brass plasmas, which did not show significant differences in harmonic spectra when comparing few-cycle pulses with fixed and random CEP. In the meantime, comparative studies with gas media under similar experimental conditions were carried out and a characteristic dependence of the HHG spectra on the CEP, commonly observed in such conditions, was revealed. Thus, the absence of the influence of the CEP on the harmonic pattern generated by few-cycle pulses from ablation plumes appears to be a common feature of plasma HHG.

9. Conclusions

Plasma HHG opens the door to many, sometimes unexpected, areas of light–matter interaction. Besides being an alternative method for generating coherent XUV radiation, it can be used as a powerful tool for various spectroscopic and analytical applications. A few of them have already emerged in plasma HHG studies in recent years. The application of doubly charged ions for high-order harmonic generation has shown a promising extension of the cut-off photon energy in plasma harmonics, without having to rely on few-cycle driving pulses. As has been shown in examining low-order harmonics, the conversion efficiency can be strongly enhanced by making use of resonances in radiative transitions of atomic or ionic systems. This has been demonstrated in pioneering plasma harmonic experiments on indium and other metals. For laser-generated plasmas, a large variety of materials can be employed, thereby increasing the chance of selecting such resonances with fixed-frequency Ti:sapphire lasers. Furthermore, it has been shown that two-color pumping profitably enhances the high-harmonic intensity and significantly influences the output and properties of the harmonic spectrum in rare gases. For plasma harmonics, where this technique has recently been adopted, this will be a new approach for the nonlinear spectroscopy of ion transitions possessing high oscillator strengths.

Future developments in the application of this technique may include such areas as the seeding of plasma resonance harmonics in XUV FELs, plasma-induced harmonic generation using few-cycle pulses with the corresponding generation of attosecond pulse trains, the application of endohedral fullerenes for plasma HHG, the joint generation of gas- and plasma-induced harmonics, the analysis of molecular structures through the study of harmonic spectra from oriented molecules in plasmas, the search for quasiphase matching schemes in plasma plumes, the tapping of a single harmonic for surface science, structural analysis of multidimensional formations in laser plasma, the generation of strong combs and single attosecond pulses, the quest for quasisolid-state HHG, the application of double-target schemes for plasma formation, the application of IR (2–5 μm) laser sources for extension of plasma harmonic cut-offs, and the analysis of plasma components through HHG.

In concluding this review, we would like to reiterate that plasma HHG could be very attractive in many unexpected areas of light–matter interaction. Besides being an alternative method for generating coherent XUV radiation, it can be used as a powerful tool for various spectroscopic and analytical applications.

Acknowledgments

The author expresses deep appreciation to his numerous colleagues with whom most of the investigations presented in this review were carried out. Special acknowledgments are due to H Kuroda, J P Marangos, J W G Tisch, P D Gupta, P A Naik, M Lane, V V Strelkov, E Fiordilino, C Hutchison, H Singhal, P V Redkin, T Usmanov, I A Kulagin, M Tudorovskaya, M Khokhlova, G S Boltaev, and N Kh Satlikov for the cooperation and fruitful discussions of different aspects of harmonic generation in laser-produced plasmas. The author acknowledges support from the Marie Curie International Incoming Fellowship Grant within the 7th European Community Framework Programme (grant No. PIIF-GA-2009-253104) and the Volkswagen Foundation (grant No. 85124).

References

1. Ganeev R A *Laser Phys.* **18** 1009 (2008)
2. Ganeev R A *Open Spectrosc. J.* **3** 1 (2009)
3. Ganeev R A *Laser Phys.* **21** 25 (2011)
4. Ganeev R A *J. Phys. B At. Mol. Opt. Phys.* **40** R213 (2007)
5. Ganeev R A *Phys. Usp.* **52** 55 (2009) [*Usp. Fiz. Nauk* **179** 65 (2009)]
6. Tsakiris G D et al. *New J. Phys.* **8** 19 (2006)

7. Dromey B et al. *Nature Phys.* **2** 456 (2006)
8. Reitze D H et al. *Opt. Lett.* **29** 86 (2004)
9. Pfeifer T et al. *Appl. Phys. B* **80** 277 (2005)
10. Froud C A et al. *Opt. Lett.* **31** 374 (2006)
11. Gibson E A et al. *Science* **302** 95 (2003)
12. Kazamias S et al. *Phys. Rev. Lett.* **90** 193901 (2003)
13. Teubner U et al. *Phys. Rev. A* **67** 013816 (2003)
14. Norreys P A et al. *Phys. Rev. Lett.* **76** 1832 (1996)
15. Pert G J *Phys. Rev. A* **75** 023808 (2007)
16. Ozaki T et al. *Phys. Rev. Lett.* **89** 253902 (2002)
17. Grüner F et al. *Appl. Phys. B* **86** 431 (2007)
18. Corkum P B, Krausz F *Nature Phys.* **3** 381 (2007)
19. Figueira de Morisson Faria C et al. *Phys. Rev. A* **65** 023404 (2002)
20. Taïeb R et al. *Phys. Rev. A* **68** 033403 (2003)
21. Silin V P, Silin P V *Phys. Usp.* **50** 729 (2007) [*Usp. Fiz. Nauk* **177** 763 (2007)]
22. Akiyama Y et al. *Phys. Rev. Lett.* **69** 2176 (1992)
23. Kubodera S et al. *Phys. Rev. A* **48** 4576 (1993)
24. Wahlström C-G et al. *Phys. Rev. A* **51** 585 (1995)
25. Theobald W et al. *Opt. Commun.* **120** 177 (1995)
26. Ganeev R A, Redkorechev V I, Usmanov T *Opt. Commun.* **135** 251 (1997)
27. Corkum P B *Phys. Rev. Lett.* **71** 1994 (1993)
28. Gladkov S M, Koroteev N I *Sov. Phys. Usp.* **33** 554 (1990) [*Usp. Fiz. Nauk* **160** (7) 105 (1990)]
29. Ganeev R et al. *Opt. Lett.* **30** 768 (2005)
30. Ganeev R A et al. *Opt. Lett.* **31** 1699 (2006)
31. Ganeev R A et al. *Phys. Rev. A* **74** 063824 (2006)
32. Ganeev R A et al. *J. Appl. Phys.* **99** 103303 (2006)
33. Ganeev R A et al. *Opt. Lett.* **32** 65 (2007)
34. Ganeev R A et al. *Appl. Phys. B* **81** 1081 (2005)
35. Ganeev R A et al. *J. Opt. Soc. Am. B* **23** 2535 (2006)
36. Suzuki M et al. *Opt. Lett.* **31** 3306 (2006)
37. Ganeev R A et al. *Phys. Rev. Lett.* **102** 013903 (2009)
38. Ganeev R A et al. *Appl. Phys. B* **87** 243 (2007)
39. Suzuki M et al. *Opt. Express* **15** 4112 (2007)
40. Ganeev R A et al. *Phys. Rev. A* **76** 023831 (2007)
41. Ganeev R A et al. *Phys. Lett. A* **339** 103 (2005)
42. Elouga Bom L B et al. *Phys. Rev. A* **75** 033804 (2007)
43. Ganeev R A et al. *Phys. Rev. A* **75** 063806 (2007)
44. Ganeev R A et al. *Phys. Rev. A* **76** 023805 (2007)
45. Ganeev R A et al. *Phys. Rev. A* **76** 023832 (2007)
46. Ganeev R A et al. *Phys. Rev. A* **80** 033845 (2009)
47. Ganeev R A et al. *Phys. Rev. A* **80** 043808 (2009)
48. Ganeev R A et al. *J. Opt. Soc. Am. B* **27** 1077 (2010)
49. Redkin P V, Ganeev R A *Phys. Rev. A* **81** 063825 (2010)
50. Ganeev R A et al. *Appl. Phys. B* **100** 581 (2010)
51. Singhal H et al. *Phys. Rev. A* **82** 043821 (2010)
52. Ganeev R A et al. *Phys. Rev. A* **82** 053831 (2010)
53. Redkin P V, Kodirov M K, Ganeev R A *J. Opt. Soc. Am. B* **28** 165 (2011)
54. Ganeev R A et al. *Phys. Rev. A* **83** 013820 (2011)
55. Ganeev R A et al. *J. Opt. Soc. Am. B* **28** 360 (2011)
56. Ganeev R A, Kuroda H *Appl. Phys. B* **103** 151 (2011)
57. Ganeev R A et al. *J. Mod. Opt.* **58** 819 (2011)
58. Ganeev R A et al. *Phys. Rev. A* **83** 063837 (2011)
59. Redkin P V, Danailov M B, Ganeev R A *Phys. Rev. A* **84** 013407 (2011)
60. Ganeev R A, Elouga Bom L B, Ozaki T *Phys. Plasmas* **18** 083101 (2011)
61. Ganeev R A et al. *Eur. Phys. J. D* **64** 109 (2011)
62. Elouga Bom L B et al. *Opt. Express* **19** 3677 (2011)
63. Pertot Y et al. *Appl. Phys. Lett.* **98** 101104 (2011)
64. Pertot Y et al. *J. Phys. B At. Mol. Opt. Phys.* **45** 074017 (2012)
65. Haessler S et al. *J. Phys. B At. Mol. Opt. Phys.* **45** 074012 (2012)
66. Ganeev R A et al. *Opt. Express* **20** 90 (2012)
67. Ganeev R A et al. *Phys. Rev. A* **85** 015807 (2012)
68. López-Arias M et al. *J. Appl. Phys.* **111** 043111 (2012)
69. Ganeev R A et al. *Phys. Rev. A* **85** 023832 (2012)
70. Suzuki M et al. *J. Phys. B At. Mol. Opt. Phys.* **45** 065601 (2012)
71. Ganeev R A et al. *Opt. Commun.* **285** 2934 (2012)
72. Hutchison C et al. *Opt. Lett.* **37** 2064 (2012)
73. Ganeev R A et al. *J. Phys. B At. Mol. Opt. Phys.* **45** 165402 (2012)
74. López-Arias M et al. *Mol. Phys.* **110** 1651 (2012)
75. Hergott J-F et al. *Phys. Rev. A* **66** 021801(R) (2002)
76. Takahashi E, Nabekawa Y, Midorikawa K *Opt. Lett.* **27** 1920 (2002)
77. Donnelly T D et al. *Phys. Rev. Lett.* **76** 2472 (1996)
78. Elouga Bom L B et al. *Appl. Phys. Lett.* **94** 111108 (2009)
79. Paul P M et al. *Science* **292** 1689 (2001)
80. Bahabad A, Murnane M M, Kapteyn H C *Nature Photon.* **4** 570 (2010)
81. Seres J et al. *Nature Phys.* **3** 878 (2007)
82. Sheinfux A H et al. *Appl. Phys. Lett.* **98** 141110 (2011)
83. Ciappina M F, Becker A, Jaroń-Becker A *Phys. Rev. A* **76** 063406 (2007)
84. Ruggenthaler M, Popruzhenko S V, Bauer D *Phys. Rev. A* **78** 033413 (2008)
85. Zhang G P *Phys. Rev. Lett.* **95** 047401 (2005)
86. Meyer H-D, Manthe U, Cederbaum L S *Chem. Phys. Lett.* **165** 73 (1990)
87. Bhardwaj V R, Corkum P B, Rayner D M *Phys. Rev. Lett.* **93** 043001 (2004)
88. Cricchio D et al *J. Phys. B At. Mol. Opt. Phys.* **42** 085404 (2009)
89. Ganeev R A et al. *J. Opt. Soc. Am. B* **30** 7 (2013)
90. Moiseyev N, Lein M *J. Phys. Chem. A* **107** 7181 (2003)
91. Zhou Z-Y, Yuan J-M *Chinese Phys. Lett.* **24** 683 (2007)
92. Millack T, Maquet A *J. Mod. Opt.* **40** 2161 (1993)
93. Gauthey F I et al. *Phys. Rev. A* **52** 525 (1995)
94. Chu W et al. *Phys. Rev. B* **82** 125301 (2010)
95. Zhou Z, Yuan J *Phys. Rev. A* **77** 063411 (2008)
96. Kapoor V, Bauer D *Phys. Rev. A* **85** 023407 (2012)
97. Di Piazza A, Fiordilino E *Phys. Rev. A* **64** 013802 (2001)
98. Bandrauk A D, Chelkowski S, Nguyen H S *J. Mol. Struc.* **735–736** 203 (2005)
99. Fano U *Phys. Rev.* **124** 1866 (1961)
100. Raseev G, Leyh B, Lefebvre-Brion H *Z. Phys. D* **2** 319 (1986)
101. Keller F, Lefebvre-Brion H *Z. Phys. D* **4** 15 (1986)
102. Amusia M Ya, Connerade J-P *Rep. Prog. Phys.* **63** 41 (2000)
103. Reintjes J F *Nonlinear Optical Parametric Processes in Liquids and Gases* (New York: Academic Press, 1984) [Translated into Russian (Moscow: Mir, 1987)]
104. Gaarde M B, Schafer K J *Phys. Rev. A* **64** 013820 (2001)
105. Toma E S et al. *J. Phys. B At. Mol. Opt. Phys.* **32** 5843 (1999)
106. Zeng Z et al. *Phys. Scripta* **66** 321 (2002)
107. Bartels R et al. *Nature* **406** 164 (2000)
108. Plaja L, Roso L *J. Mod. Opt.* **40** 793 (1993)
109. Milošević D B *J. Phys. B At. Mol. Opt. Phys.* **40** 3367 (2007)
110. Kulagin I A, Usmanov T *Opt. Lett.* **34** 2616 (2009)
111. Strelkov V *Phys. Rev. Lett.* **104** 123901 (2010)
112. Milošević D B *Phys. Rev. A* **81** 023802 (2010)
113. Frolov M V, Manakov N L, Starace A F *Phys. Rev. A* **82** 023424 (2010)
114. Tudorovskaya M, Lein M *Phys. Rev. A* **84** 013430 (2011)
115. Frolov M V et al. *Phys. Rev. Lett.* **102** 243901 (2009)
116. Minemoto S et al. *Phys. Rev. A* **78** 061402(R) (2008)
117. Wörner H J et al. *Phys. Rev. Lett.* **102** 103901 (2009)
118. Agostini P, DiMauro L F *Rep. Prog. Phys.* **67** 813 (2004)
119. Krausz F, Ivanov M *Rev. Mod. Phys.* **81** 163 (2009)
120. Runge E, Gross E K U *Phys. Rev. Lett.* **52** 997 (1984)
121. Marques M A L et al. *Comput. Phys. Commun.* **151** 60 (2003)
122. Castro A et al. *Phys. Status Solidi B* **243** 2465 (2006)
123. Marques M A L, Gross E K U *Lecture Notes Phys.* **620** 144 (2003)
124. Ganeev R A et al. *J. Opt. Soc. Am. B* **28** 1055 (2011)
125. Duffy G, van Kampen P, Dunne P *J. Phys. B At. Mol. Opt. Phys.* **34** 3171 (2001)
126. Cowan R D *The Theory of Atomic Structure and Spectra* (Berkeley: Univ. of California Press, 1981)
127. Lide D R (Ed.) *CRC Handbook of Chemistry and Physics* 73rd ed. (Boca Raton: CRC Press, 1992)
128. Strelkov V V et al. *J. Phys. B At. Mol. Opt. Phys.* **39** 577 (2006)
129. Ganeev R A et al. *Opt. Express* **20** 25239 (2012)

130. Feit M D, Fleck J A (Jr.), Steiger A *J. Comput. Phys.* **47** 412 (1982)
131. Kjeldsen H et al. *J. Phys. B At. Mol. Opt. Phys.* **37** 1321 (2004)
132. Gabor D *J. IEE Radio Commun. Eng.* **93** 429 (1946)
133. Altucci C, Tisch J W G, Velotta R *J. Mod. Opt.* **58** 1585 (2011)
134. Chipperfield L E et al. *J. Mod. Opt.* **52** 243 (2005)
135. Goulielmakis E et al. *Science* **320** 1614 (2008)
136. Ganeev R A *Laser Phys. Lett.* **9** 175 (2012)
137. Ganeev R A *Laser Phys.* **22** 1177 (2012)
138. Ganeev R A et al. *J. Opt.* **14** 095202 (2012)
139. Ganeev R A *J. Mod. Opt.* **59** 409 (2012)
140. Yao J et al. *J. Mod. Opt.* **59** 245 (2012)
141. Ferray M et al. *J. Phys. B At. Mol. Opt. Phys.* **21** L31 (1988)
142. Lompré L A et al. *J. Opt. Soc. Am. B* **7** 754 (1999)
143. McPherson A et al. *J. Opt. Soc. Am. B* **4** 595 (1987)
144. Borot A et al. *Opt. Lett.* **36** 1461 (2011)
145. Torres R et al. *Opt. Express* **18** 3174 (2010)
146. Vozzi C et al. *Appl. Phys. Lett.* **86** 111121 (2005)
147. Tate J et al. *Phys. Rev. Lett.* **98** 013901 (2007)
148. Schiessl K et al. *Phys. Rev. Lett.* **99** 253903 (2007)
149. Witting T et al. *Opt. Lett.* **36** 1680 (2011)
150. Robinson J S et al. *Appl. Phys. B* **85** 525 (2006)
151. Sanz M et al. *J. Nanopart. Res.* **13** 6621 (2011)
152. Torres R, Jadraque M, Martin M *Appl. Phys. A* **80** 1671 (2005)
153. Anselment M et al. *Chem. Phys. Lett.* **134** 444 (1987)
154. Rohlfing E A *J. Chem. Phys.* **89** 6103 (1988)
155. Acquaviva S, De Giorgi M L *Appl. Surf. Sci.* **197 – 198** 21 (2002)
156. Roth J, Gähler F, Trebin H-R *Int. J. Mod. Phys. C* **11** 317 (2000)
157. Glover T E *J. Opt. Soc. Am. B* **20** 125 (2003)
158. Jeschke H O, Garcia M E, Bennemann K H *Phys. Rev. Lett.* **87** 015003 (2001)
159. Kabashin A V, Meunier M *J. Appl. Phys.* **94** 7941 (2003)
160. Creasy W R, Brenna J T *Chem. Phys.* **126** 453 (1988)
161. O'Brien S C et al. *J. Chem. Phys.* **88** 220 (1988)
162. Donnelly T D et al. *Phys. Rev. Lett.* **76** 2472 (1996)
163. Tisch J W G et al. *J. Phys. B At. Mol. Opt. Phys.* **30** L709 (1997)
164. Altucci C et al. *Phys. Rev. A* **61** 021801(R) (2000)
165. Froud C A et al. *Opt. Lett.* **31** 374 (2006)
166. Kim S et al. *Nature* **453** 757 (2008)
167. Husakou A, Im S-J, Herrmann J *Phys. Rev. A* **83** 043839 (2011)
168. Kjeldsen H et al. *J. Phys. B At. Mol. Opt. Phys.* **37** 1321 (2004)
169. Marr G V, West J B *Atom. Data Nucl. Data Tabl.* **18** 497 (1976)
170. Levesque J et al. *Phys. Rev. Lett.* **98** 183903 (2007)
171. Shiner A D et al. *Nature Phys.* **7** 464 (2011)
172. Ganeev R A et al. *Appl. Phys. Lett.* **94** 051101 (2009)
173. Hentschel M et al. *Nature* **414** 509 (2001)
174. Witting T et al. *J. Phys. B At. Mol. Opt. Phys.* **45** 074014 (2012)
175. Altucci C, Tisch J W G, Velotta R *J. Mod. Opt.* **58** 1585 (2011)
176. Kilbane D et al. *J. Phys. B At. Mol. Opt. Phys.* **38** L1 (2005)
177. Dolmatov V K *J. Phys. B At. Mol. Opt. Phys.* **29** L687 (1996)
178. West J B et al. *J. Phys. B At. Mol. Opt. Phys.* **36** L327 (2003)